Study on Effectiveness of Magnetic Field Assisted Flushing in Improvement of Process Parameters in Electrical Discharge Machining

MAKENZI M. MACBEN

MASTER OF SCIENCE

(Mechatronic Engineering)

JOMO KENYATTA UNIVERSITY OF AGRICULTURE AND TECHNOLOGY

2012

DECLARATION

This thesis is my original work and to the best of my knowledge, it has not been presented for a degree award in this or any other university.

Signature..... Date.....

Makenzi Macben Mutua

Reg No: EN392-1587/2010

This thesis has been submitted for examination with our approval as the University supervisors:

Signature..... Date.....

Prof.Eng. Ikua. B.W

Signature..... Date.....

Prof. Nyakoe. G.N

DEDICATION

This work is dedicated to my parents Dr. and Mrs. Makenzi, for standing by me all through my academic and career pursuits.

ACKNOWLEDGEMENT

All glory goes to the Almighty God for enabling me to successfully complete this academic pursuit.

This research was carried out at the department of Mechatronic Engineering, Jomo Kenyatta University of Agriculture and Technology(JKUAT). It was sponsored by the same institution and as such their support is hereby gratefully acknowledged.

I would like to sincerely thank my supervisors, Prof.Eng. Ikua B.W and Prof.Nyakoe G.N for their invaluable guidance, support and advice on both this research undertaking and also on my career endeavours.

I would like to acknowledge and appreciate Mr. S.Ngige and Mr.M.Waweru of Diemould Machinery Product and Services Industry (DPMS) and Mr N.M.Shiyonga and Mr J.N.Njeru of the National Youth Service(NYS). Without their facilitation with key equipments, this research would not have been possible.

Special thanks goes to Mr. K. Kabini, E.Wangui and E.Murimi for their ready assistance; Mr. S. Nzioka and Mr. M. Mumu for their technical advice in the use of the departmental facilities. I express my sincere thanks to all members of staff and my colleagues in Mechanical and Mechatronic Engineering departments for their contribution to my work through their comments, constructive criticism, suggestions and their encouragement.

I would like to express great gratitude to my parents Paul and Margaret Makenzi and my siblings Rose and Brian whose guidance, prayers, encouragement and overall support ensured that I was able to successfully undertake and complete this research.

Contents

List of Figures

List of Tables

ABBREVIATIONS

AJM	Abrasive jet machining
ANOVA	Analysis of variance
CCD	Central composite design
EBM	Electron beam machining
ECM	Electrochemical machining
EDM	Electrical discharge machining
EWR	Electrode wear rate
GAME	Gravity Assisted Micro-EDM
HDDR	Hydrogen disproportionation desorption recombination
LBM	Laser beam machining
MAF	Magnetic abrasive finishing
MAFF	Magnetic abrasive flow finishing
MMF	Magnetomotive force
MS	Mean Square
MRR	Material removal rate
P	Permeance
RSM	Response Surface Methodology
SS	Sum of Squares
TWR	Tool Wear Rate
USM	ULtrasonic machining
WJM	Water jet machining

NOMENCLATURE

B	Magnetic flux density (Wb/m^2)
BH_{max}	Maximum energy product (MGOe)
E	Electric field strength (NC^{-1})
H_{ci}	Coercivity (Oe)
I_p	Single-pulse current (A)
M	Magnetic intensity (G)
MGOe	Megagauss oersted
M_r	Remanence (T)
Oe	Oersted
q	Ion Charge (C)
T	Teslas
T_c	Curie temperature
T_n	Pulse-on time (μ s)
T_{off}	Pulse-off time (μ s)
V_p	Single-pulse voltage (V)
v	Velocity (ms^-1)
μ	Fluid viscosity (Pa s)
μ_r	relative permeability
ρ	Fluid density
b	Drag co-efficient
Δp	Particle magnetic susceptibility
Δm	Medium magnetic susceptibility

ABSTRACT

Electrical-discharge machining (EDM) is an electrothermal process for machining geometrically complex and/or hard material components such as heat treated tool steels, composites and super alloys. It is widely used in die and mold making, aeronautics and nuclear industries.

The accumulation of debris at the spark gap region can affect the effeciency and overall outcome of the machining process. The material removal rate, tool wear and surface roughness are all dependent on conditions at this region.

Occurrence of short-circuits and arcing between the workpiece and tool electrode is a challenge faced during EDM operations. These conditions are detrimental as they greatly compromise the machining efficiency and quality of the process. The eroded debris can cause a short circuit at the spark gap. When this occurs, there is no material removal and there is risk of the tool welding on to the workpiece. Arcing may also occur when a portion of the cavity contains too many eroded debris and the electric current is discharged through them. This leads to poor surface finish and reduced material removal rate and tool life. Therefore, there is need for an efficient mechanism for optimum clearing of the spark gap of all eroded debris.

This research investigated the effectiveness of the use of magnetic energy in removal of debris from the spark gap and the influence of application of varied levels of magnetic intensity on the various performance parameters of the EDM process. Empirical modelling and surface response methods were used for the analysis of these parameters.

It was found that the introduction of magnetic force in the spark-gap region improved the process parameters by increasing the rates of material removal and reducing the surface roughness and tool wear rate.

Chapter 1

INTRODUCTION

1.1 Overview

Electrical-discharge machining (EDM) also referred to as spark machining or spark erosion is a controlled material-removal process that is used in machining of metals by means of electric sparks. It is widely used in the manufacture of dies, punches and moulds, finishing parts for aerospace and automotive industry, and surgical components [1]. This process is employed on electrically conductive workpieces irrespective of their hardness or brittleness [2] .

It is a machining method primarily used for hard metals or those that would be difficult to machine with traditional techniques such as milling, drilling or grinding [3]. It is used on electrically conductive materials, although methods for machining insulating ceramics with EDM have also been proposed [4]. EDM can be used to cut intricate contours or cavities in pre-hardened steel without the need for heat treatment to soften them during machining. This method can be used with metal or metal alloys such as titanium, hastelloy, kovar, and inconel. Application of this process to shape polycrystalline diamond tools has also been reported [5].

In EDM technique, material is removed from the workpiece by a series of rapidly recurring current discharges between two electrodes (the tool and the workpiece) separated by a dielectric liquid and subjected to an electric voltage. Generally, kerosene or de-ionised water is used as the dielectric medium. The tool is connected to the negative terminal of the spark generator and the workpiece is connected to the positive terminal. Figure 1.1 shows the basic working principle of the EDM process.

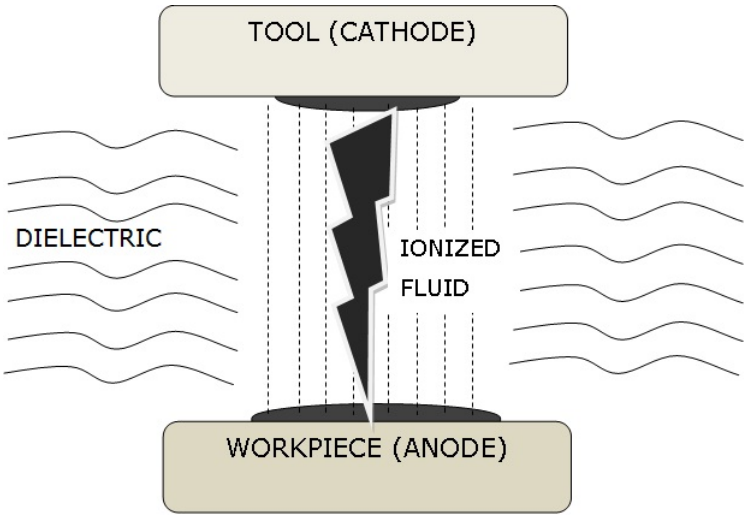

Figure 1.1: Working principles of EDM

The electric field established between the tool electrode and workpiece electrode accelerates electrons emitted from the tool towards the workpiece through the dielectric medium and the high speed electrons then impinge on the workpiece. The kinetic energy of the electrons and ions on impact with the surface of the job and tool respectively are converted into thermal energy or heat flux. Such intense localised heat flux leads to rise in temperature in excess of 10,000°C. This localised rise in temperature leads to instant vaporization/melting of the material and thus material removal.

Arcing and short-circuiting are detrimental phenomena that are sometimes experienced in the EDM process especially if the control system of the electrode fails to react quickly enough to prevent the two electrodes from getting into contact. Presence of debris within the spark-gap region may also lead to short-circuiting if the flushing action is inadequate to restore the insulating properties of the dielectric fluid. The presence of debris can also lead to current always discharging at the point of the inter-electrode volume (this is referred to as arcing), with a

consequent unwanted change of shape (damage) of the tool-electrode and workpiece.

1.2 Problem statement

The gap conditions of electrical-discharge machining significantly affects the stability of machining process. Arcing occurs when a portion of the cavity contains too many eroded particles, which facilitate the passage of electric current through them. This leads to unwanted cavities, results in poor surface finish of the job and reduced material removal rate and tool life.

Short-circuits occur when the electrode makes contact with the workpiece. There is no material removal during this occurrence and there is a risk of welding of the tool onto the workpiece. Therefore, it is necessary to ensure that the spark gap region is cleared of all eroded debris in order to enhance machining efficiency and quality of the workpiece.

Existing flushing systems such as jet, pressure and suction flushing utilize dielectric fluid only as a means of removing eroded debris from the spark gap. This results in partial clearing of eroded debris as opposed to complete and efficient clearing of the same. There is therefore, need for an effective means of debris removal to improve the EDM performance parameters. The use of a magnetic field has been proposed as an alternative for flushing

This research investigated the effectiveness of magnetic field force in removal of debris from the spark gap.

1.3 Research objectives

The main objective of this research was to investigate the effectiveness of magnetic field in removal of debris and enhancement of performance parameters in Electrical Discharge Machining.

The tasks of the research included:

- To design and fabricate a variable magnetic field force setup for debris dispersal and circulation.
- To investigate the effects of magnetic intensity, pulse-on and pulse-off time and current on the material removal rate, surface roughness and tool wear rate and to establish optimal machining conditions.
- To generate and analyse empirical models relating material removal rate, tool wear rate and surface roughness to magnetic field intensity, pulse-on and pulse-off time and current.

1.4 Significance of the study

The results of this research will be useful in the improvement of the efficiency and quality capabilities of electrical discharge machines through optimization of the process parameters. The knowledge gained will contribute towards development of literature on various aspects of electrical discharge machining focusing on spark gap conditions and improvement of the process as a whole. This is vital considering the research addresses a new approach of process optimization in EDM.

Chapter 2

LITERATURE REVIEW

2.1 Overview

Metal erosion by spark discharges was first noted by Sir Joseph Priestly in 1768 [6]. In 1943, Lazarenko conducted investigations on the reduction of wear on electric power contacts [7]. It was deduced that spark discharges could be utilized for machining metals which were proving difficult to machine using conventional methods. Lazarenko developed an EDM machining process for difficult-to-cut metals. Their system used the Resistor-Capacitor (RC) type of power supply, a system that was widely adopted in the EDM machines in the 1950s.

McGeough [8] explained the concept of spark erosion using contact breaker points and the sparking plug electrodes in car engines. He outlined the nature of the various classes of electrical discharges -the high voltage capacitative spark discharge, the normal arc discharge, and the low voltage arc that occurs at electrical contacts-

In the EDM operations, both the workpiece and tool electrode are made of electrically conducting materials. Materials commonly used as tool electrodes include brass, graphite, copper, tungsten carbide and alloys of copper.

Town [9] demonstrated that conventional methods of removing materials from workpieces are not readily applicable to new materials developed with increased hardness, strength and high-temperature resistance.

EDM has the following advantages over conventional machine tools [10]:

- It can produce complex shapes and sections accurately, faster and at lower costs.

- It can machine hardened workpieces without deforming them.
- It can machine thin fragile sections such as webs or fins easily without deforming the part.
- The process is burr-free.

2.2 Mechanism of material removal in Electrical-discharge machining

During electrical-discharge machining, an electric field is established in the gap depending on the applied potential difference and the distance between the tool electrode and workpiece electrode. When the potential difference between the electrodes is high enough, cold emission occurs. The emitted electrons are then accelerated towards the workpiece through the dielectric medium. As these electrons gain velocity, collisions occur between them and dielectric molecules, resulting in ionisation of the dielectric molecules. As the electrons are accelerated, more positive ions and electrons are generated due to collisions. This process results in a pool of electrons and ions in the dielectric medium between the tool and the job at the spark gap. Over time, the concentration becomes so high that plasma forms. The electrical resistance of such plasma channel is very small, and therefore, instantaneously, a large number of electrons flows from the tool to the job and ions from the job to the tool. This avalanche motion of electrons and ions can be visually seen as a spark. The electrical energy is dissipated as the thermal energy of the spark [11]. The kinetic energy of the electrons and ions on impact with the surface of the job and tool respectively is converted into thermal energy which causes melting and consequently material removal.

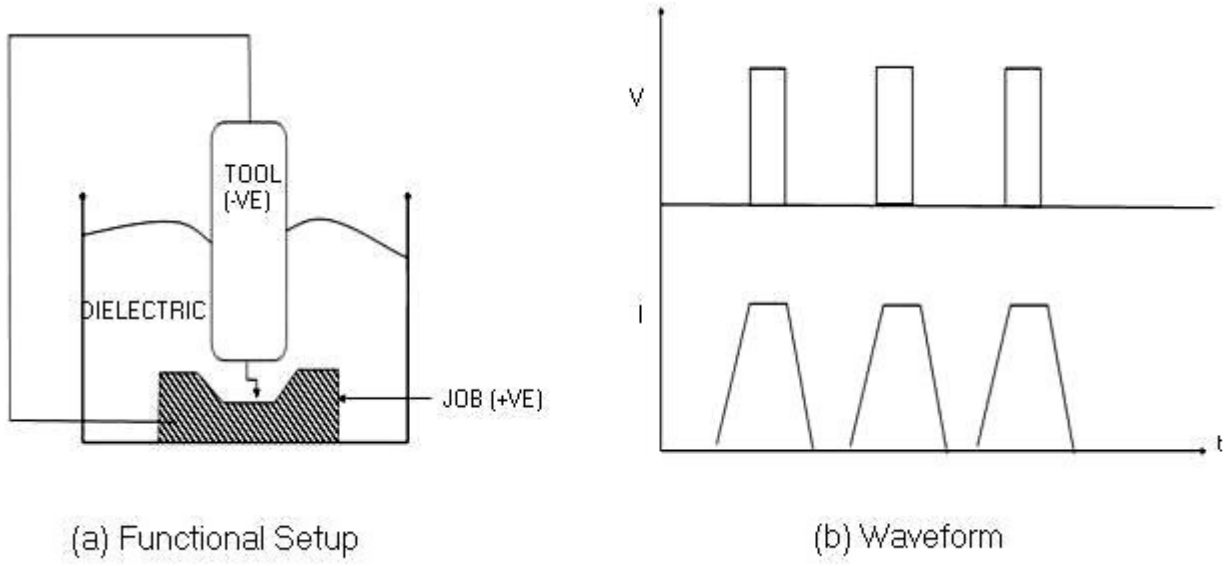

Figure 2.1: Schematic representation of the basic working principle of EDM process.

As the potential difference is withdrawn during the intervals indicated in Figure 2.1b, the plasma channel is no longer sustained and therefore it collapses generating pressure or shock waves, which evacuate the molten material forming a crater of removed material (debris) around the site of the spark [12].

2.3 Debris removal mechanisms

In the EDM process, various sizes of discharge craters are formed on the machined surface on removal of material, and the surface quality of the machined surface is governed by the size of these craters. In addition, the machining debris suspended within the dielectric fluid can accumulate in the machining gap and induce abnormal electrical discharge, thus affecting the stability of EDM progress. Therefore, if the debris in the machining gap can be removed effectively and completely, the EDM process can attain high efficiency, high precision, and high-quality surfaces.

The machining efficiency and the quality of surface associated with EDM processes are directly affected by the ability to remove machined debris from the spark gap. Several researchers have investigated the effects of dielectric flush and ejection mechanisms of machining debris for EDM. Rajurkar *et al.* [13] developed a model for debris ejection mechanism based on shock waves resulting from electrical discharge. Masuzawa *et al.* [14] investigated a dynamic jet flushing method and showed that the sweeping jet method was superior to conventional fixed-jet flushing.

For further improvement in the expelling of debris to prevent clogging in the machining gap, several researchers have carried out studies on ultrasonic vibration through either tool electrode or workpiece electrode, as well as dielectric fluid to prevent debris accumulation and to maintain the stability of the machining progress [15, 16]. These studies revealed that preventing debris accumulation in the machining gap had the benefit of improving machining efficiency. Furthermore, the added abrasives that acted as ultrasonic media for the combined process of EDM with ultrasonic machining(USM) can be regarded as the surface strengthening agents transferred to the machined surface through ionization of discharge column during the process [17].

The combined process of EDM with USM has the potential to prevent debris accumulation, improve machining efficiency and improve the machined surface. However, to design an USM equipment for machining large area is rather difficult. Other methods of clearing the spark gap are thus being investigated.

2.4 Overview of flushing methods

Flushing is the process of removing debris from the spark gap. It is a very important function in any electrical-discharge machining operation. The dielectric fluid serves a vital role in flushing [18], in addition to the following functions:

- It helps in initiating discharge by serving as a conducting medium when ionised, and conveys the spark.
- It helps in quenching the spark and cooling the work and tool electrode.

The electrode wear rate, metal removal rate and other performance characteristics are also influenced by the dielectric fluid [3]. Typical dielectric fluids include transformer oil, silicon oil, kerosene and de-ionized water. The dielectric fluid should posses certain characteristics which include: high dielectric strength and quick recovery after breakdown, effective quenching and flushing ability.

Schumacher [19] reported that too much debris in the discharge gap often causes a continuous arc and/or short circuit and makes the process unstable.

Efficient flushing requires a balance between pressure of dielectric fluid and volume. For roughing operations, where there is a much larger gap, high volume of dielectric and low pressure flushing is advised. On the other hand, in finishing operations, the arc gap is much smaller and thus higher pressures are required to ensure proper dielectric flow.

There are four types of flushing techniques namely:

1. Pressure flushing

2. Suction flushing

3. Jet flushing

4. Pulse flushing

Pressure and suction flushing are categorized as direct flushing techniques while jet and pulse flushing are categorized as indirect flushing techniques. Pressure and Jet flushing techniques are the most commonly used flushing techniques and are therefore discussed below.

2.4.1 Pressure flushing

Pressure flushing, also referred to as injection flushing is the most common method of flushing. It can be performed through the tool or through the workpiece. Figure 2.2a shows pressure flushing through the tool [14].

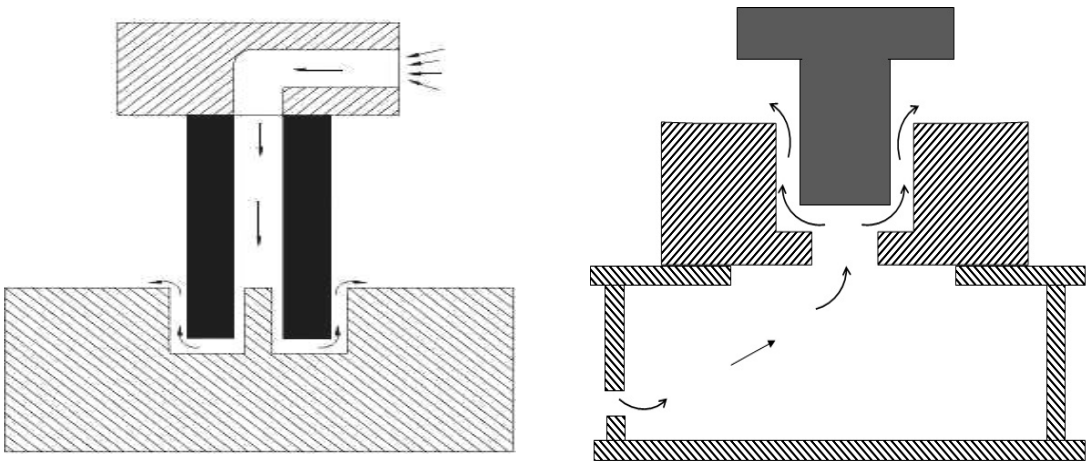

(a) Normal pressure flushing (b) Pressure flushing through the workpiece

Figure 2.2: Pressure flashing

Figure 2.2b shows pressure flushing done by forcing the dielectric fluid through the workpiece

mounted over a flushing pot. The advantage of this method is that it eliminates the need for holes in the electrode. Flow conditions must be properly regulated in these two methods of flushing otherwise machining conditions may be unstable with reduced removal rate and uneven tool wear. The flow velocity can be monitored by measuring the differential pressure or volume throughput.

Li and Lee [20] reported that material removal rate (MRR) decreases gradually with the flushing pressure. Improper settings of control factors in EDM injection flushing method may result in poor process performance, increased in-process variability and decrease in the manufacturability of products and processes.

The disadvantage of pressure flushing is that there is danger of a secondary discharge machining, which occurs as the eroded particles pass between the walls of the electrode and the workpiece. Figure 2.3 shows the effect of secondary discharge on the workpiece [14].

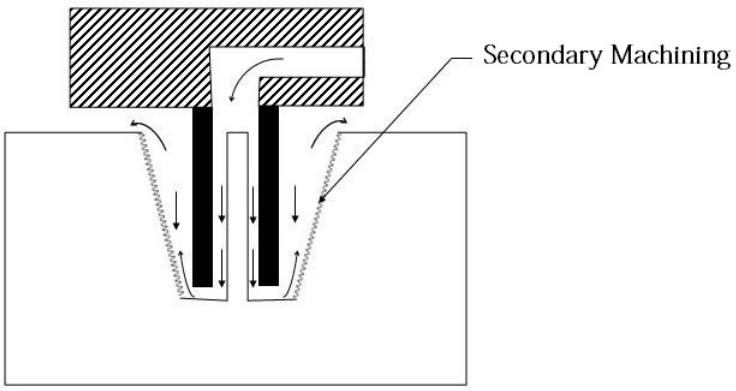

Figure 2.3: Secondary discharge as a result of pressure flushing

2.4.2 Jet flushing

Jet flushing is the simplest and oldest flush-method for EDM. A dielectric fluid jet is ejected from a nozzle (or several nozzles) towards the machining area. The pressure of the jet creates flow in the discharge gap and this flushes the debris out of the gap [14].

This method, illustrated in Figure 2.4, is very widely used because of its simplicity and good debris removal capability.

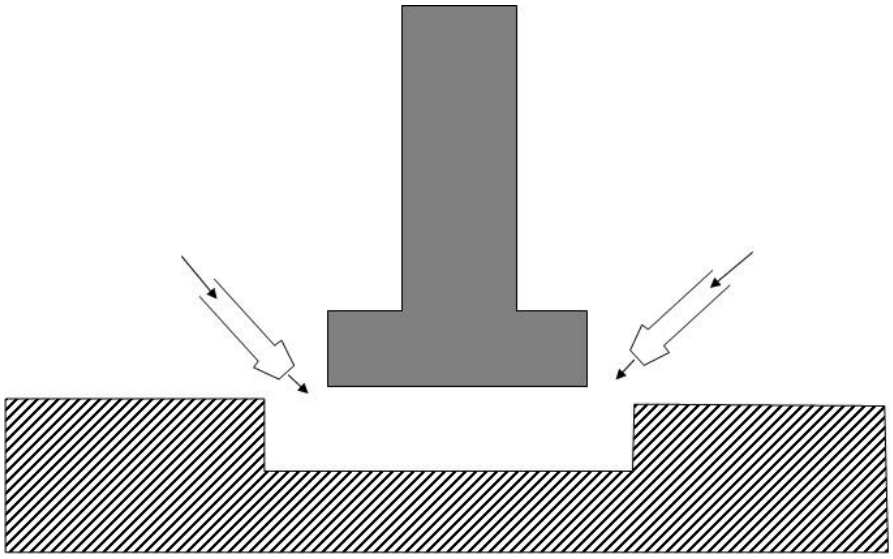

Figure 2.4: Jet flushing

However, it is not easy to determine the most appropriate position of the nozzle(s). This position is usually decided by the operators based on experience. This method however, does not ensure uniform debris dispersal because the flow in the gap is almost fixed since the nozzle is fixed at a certain position [15].

Inspite of the above problems, the simplicity of this method makes it attractive, and if the position of the nozzle is adjustable and can be controlled during machining, a new technique of flushing can be explored.

2.5 Magnetic field assistance in EDM

Magnetic field has been extensively used in non-traditional manufacturing process. Magnetic abrasive finishing (MAF) and magnetic abrasive flow finishing (MAFF) are effective methods for producing a mirror surface on metal, ceramic and composite materials [21, 22]. In recent years, researchers have used the magnetic field in electrolytic finishing process [23]. It has been reported that using magnetic field changes the ion migration paths from linear to cycloid motion. Brujin *et al.* [24] investigated the effects of magnetic field in gap cleaning and indicated that the magnetic field can improve the gap cleaning process.

Lin and Lee [25] used the magnetic field in EDM process and reported that the magnetic force removes the debris away from machining gap and improves the characteristics of this operation especially in high discharge energy regime.

Yeo *et al.* [26] drew the following conclusions from a study involving application of a magnetic field on hardened tool steel using the rotatable micro electrical-discharge machining (micro EDM) process:

(a) The presence of a magnetic field in the machining zone improves the debris removal and hence the aspect ratio of micro holes. The hole depth achieved is 26 percent higher when compared to the conventional micro EDM process under similar working conditions.
(b) The presence of the magnetic field causes some distortion in the tool electrode and increases the wear along the length of the tool electrode.
(c) The presence of the magnetic field does not affect the surface roughness values significantly.

He further noted that in the initial stages of the machining, there was no appreciable difference in the hole depth machined with and without the magnetic field. As the holes made in this short period of time are relatively shallow with an aspect ratio of less than 1, the centrifugal force alone is sufficient for the debris removal. However, with deeper holes and incresed machining durations, the effect of the magnetic field becomes clearer. Figure 2.5 shows magnetic field inside a hole when the magnet is at the top of the hole and produces a homogeneous external field.

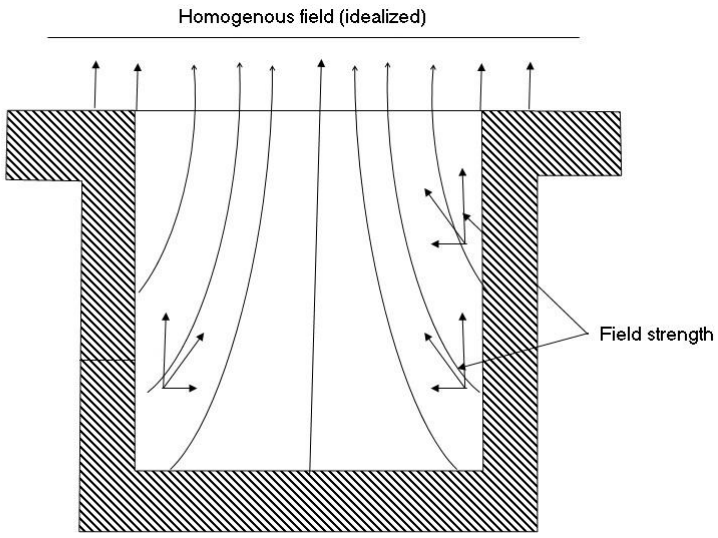

Figure 2.5: Magnetic field established inside a hole

In the absence of debris, fresh work material is continuously being exposed for sparking and hence greater hole depth is achieved [24].

The current research varied from the aforementioned work in that it was not on a micro-scale; implying the magnetic field utilized was of higher magnitude. The electrode was not rotary but traversed only longitudinally. Also, the setup incorporates a jet flushing system.

2.6 Particle and Ion Dynamics in Magnetic Field

A significant part of this research encompasses the motion of eroded ferromagnetic particles produced in electrical discharge machining in a gradient magnetic field considering the effects of fluidic forces on particles in the system.

Navier-stokes equations describe the motion of fluid substances. These equations arise from applying Newton's second law to fluid motion, together with the assumption that the fluid stress is the sum of a diffusing viscous term (proportional to the gradient of velocity), plus a pressure term.

In the general form the Navier-stokes equation is written as :

$$\rho\left(\frac{\delta \mathrm{v}}{\delta t} + \mathrm{v} \bigtriangledown \mathrm{v}\right) = \bigtriangledown \mathrm{p} + \bigtriangledown \mathrm{T} + \mathrm{f} \tag{2.1}$$

where v is the flow velocity, ρ is the fluid density, p is the pressure, T is the deviatoric stress tensor, f represents body forces per unit volume acting on the fluid and $\bigtriangledown$ is the del operator.

A simplification of the flow equation can be done when considering an incompressible flow of a newtonian fluid. It can then be restated as Equation 2.2

$$\rho\left(\frac{\delta \mathrm{v}}{\delta \mathrm{t}} + \mathrm{v} \bigtriangledown \mathrm{v}\right) = \bigtriangledown \mathrm{p} + \mu \bigtriangledown^{2} \mathrm{T} + \mathrm{f} \tag{2.2}$$

The shear stress term $\bigtriangledown$ T becomes the quantity $\mu \bigtriangledown^2 \mathrm{T}$ when the fluid is assumed incompressible, homogeneous and Newtonian, where μ is the dynamic viscosity.

The force on a magnetic particle inside a magnetic field depends on the volume of the particle (V), the difference in magnetic susceptibilities, Δx , between the particle and surrounding buffer medium, as well as the strength and gradient of the applied magnetic field. The relationship is stated in Equation 2.3

$$F_{mag} = \frac{V\Delta \mathrm{x}}{\mu}(B\bigtriangledown)B \tag{2.3}$$

The term Δx is the difference in magnetic susceptibility between the magnetic particle and its surrounding buffer or medium.

Hydrodynamic forces on moving particles are described by Stoke's Law. Drag force can be obtained as follows:

$$F_{drag} = -bv \tag{2.4}$$

Where b is the drag coefficient. The drag coefficient depends on the size and shape of the object and the viscosity of medium.

In this research, the objects are taken to be spherical particles of radius r, the drag coefficient is thus obtained according to Equation 2.5.

$$b = 6\pi\mu \mathrm{r} \tag{2.5}$$

Where μ is fluid viscosity. The velocity v of a particle following application of magnetic force is described by the differential equation (neglecting the effect of gravity and buoyancy):

$$\frac{\delta\nu}{\delta t} = \frac{F_{mag} - 6\pi\mu \mathrm{rv}}{m_p} \tag{2.6}$$

Where m_p is the mass of the particle.

2.6.1 Ion path

The plasma channel consists of electrons and positive-charged ions. When a magnetic field is applied, it will affect charged ions due to Lorentz force (force which arises due to association of magnetic and electric fields). Therefore, magnetic field may change the ions movement and lead to more collisions between ions as shown in Figure 2.6.

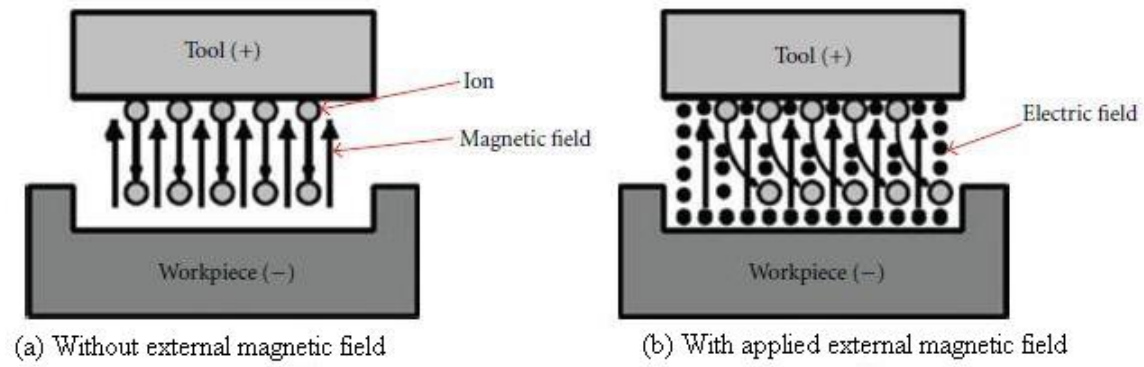

Figure 2.6: Ion path motion in gap space

This may lead to an increase in the plasma channel temperature and result in its expansion, depending on the intensity of the field. The motion of charged particles driven by magnetic field is described by the following equation:

$$\frac{\delta \mathrm{v}}{\delta \mathrm{t}} = \frac{\mathrm{q}}{\mathrm{m}}(\mathrm{E} + \mathrm{v}B) \tag{2.7}$$

Where m and q represent the mass and charge of ion, respectively. E is the electrical field

strength, B is the magnetic flux density, and v is the ion velocity.

The magnetic field that is perpendicular to an electric field changes the path of ionic movement to cycloid curve due to Lorentz force. The equation of motion of the ions is as follows;

$$\mathrm{v}_x(t) = \frac{V_g}{Bl}\sin\left(\frac{\mathrm{q}B}{m}t\right) + \mathrm{v}_x\,(0)\sin\left(\frac{\mathrm{q}B}{m}t\right) \tag{2.8}$$

$$\mathrm{v}_y(t) = \frac{V_g}{Bl}\left(1-\cos\left(\frac{\mathrm{q}B}{m}t\right)\right) + \mathrm{v}_x\,(0)\sin\left(\frac{\mathrm{q}B}{m}t\right) + \mathrm{v}_y\,(0) \tag{2.9}$$

where v_x and v_y are the velocity of ions in x and y directions. $\mathrm{v}_x(0)$ and $\mathrm{v}_y(0)$ represent the initial velocity of ions in x and y directions. V_g is the gap voltage and l is gap distance. The path equation of the ions can then be described as:

$$\mathrm{x} = \frac{mV_g}{qB^2l}\left(1-\cos\left(\frac{\mathrm{q}B}{m}t\right)\right) + \frac{m}{\mathrm{q}B} + \mathrm{v}_x\,(0)\sin\left(\frac{\mathrm{q}B}{m}t\right) + \mathrm{x}_0 \tag{2.10}$$

$$\mathrm{y} = -\frac{mV_g}{\mathrm{q}B^2l}\sin\left(\frac{\mathrm{q}B}{m}t\right) + \frac{m}{\mathrm{q}B}\mathrm{v}_x(0)\left(1-\cos\left(\frac{\mathrm{q}B}{m}t\right)\right) + \left(\frac{V_g}{Bl} + \mathrm{v}_x(0)\right)t + \mathrm{y}_0 \tag{2.11}$$

where x and y represent the trace location of the ion and x_0 and y_0 represent the initial position of the ions in electrical discharge regime.

2.7 Neodymium magnets

In order to establish the external magnetic field around the tool-workpiece system, neodymium magnets will be used.

The advent of neodymium iron boron magnets in the early 1980s was met with great enthusiasm [27]. Compared to samarium cobalt magnets of the day, the simultaneous increase in energy product and reduction in raw material cost of neodymium magnets was seen as breakthrough technology [28].

The tetragonal $Nd_2Fe_{14}B$ crystal structure has exceptionally high uniaxial magnetocrystalline anisotropy (HA 7 teslas). This gives the compound the potential to have high coercivity. The compound also has a high saturation magnetization (Js =1.6 T or 16 kG) and typically 1.3 T. Therefore, as the maximum energy density is proportional to the square of the saturation, this magnetic phase has the potential for storing large amounts of magnetic energy (BHmax 512 kJ/m^3 or 64 MGOe) [29].

Neodymium magnets have higher remanence, much higher coercivity and energy product, but often lower Curie temperature than other types of magnets. Neodymium is alloyed with terbium and dysprosium in order to preserve its magnetic properties at high temperatures.

These qualities made Neodymium-type magnets, suitable for this particular research.

2.8 EDM process and machining parameters

Some of the process parameters of particular interest in Electro-Discharge Machining include:

1. Material removal rate
2. Electrode wear ratio
3. Surface roughnes

A description of each of these process parameters is outlined below.

2.8.1 Material Removal Rate

Material removal rate (MRR) is the amount of material removed from a workpiece per unit time. It is the rate at which erosion from the workpiece takes place and is an important indicator of the efficiency and cost effectiveness of the EDM process. A mathematical model of a hemisphere can be used to represent the dimensions of a molten crater so as to be able to explain the amount of energy expended to erode a crater per spark [30]. This is illustrated in Figure 2.7.

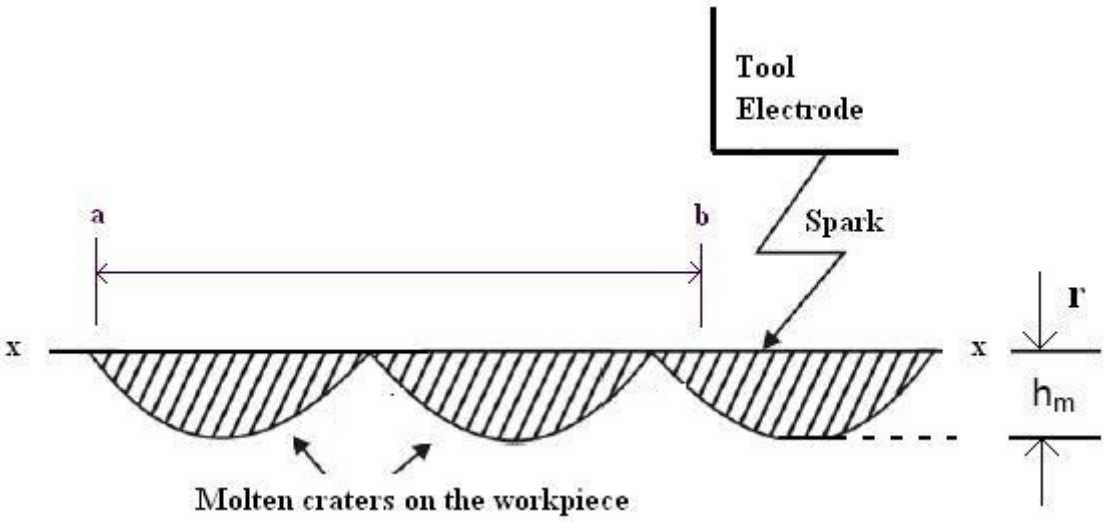

Figure 2.7: Schematic representation of craters in EDM process

Assuming that Material removed (M_r) in a single spark would be proportional to the spark energy (E_i), given by,

$$E_i = V_p I_p t_{on} \tag{2.12}$$

then,

$$M_r = \alpha V_p I_p t_{on} \tag{2.13}$$

Where;

V_p =Voltage of a single pulse,

I_p =Current of a single pulse,

t_{on} =Pulse-on time,

t_{off} =Pulse-off time.

α =Removal constant of a material (removal volume of a material per unit electric power)

Hence, the Material Removal Rate (MRR) on the workpiece is given by material removed in unit time as shown by equation 2.14 as:

$$MRR = \alpha V_p I_p t_{on} \frac{1}{t_{on} + t_{off}} \tag{2.14}$$

2.8.2 Electrode Wear Ratio

Electrode wear ratio (EWR) refers to the ratio of the wear weight of the electrode to the wear weight of the workpiece [31]. It is expressed as a percentage as shown by equation 2.15.

$$EWR = \frac{Wear\ \ weight\ \ of\ \ the\ \ electrode}{wear\ \ weight\ \ of\ \ workpiece} \times 100 \tag{2.15}$$

2.8.3 Surface Roughness

Surface roughness is a measure of the finely spaced surface irregularities on the surface of a machined workpiece. There are various methods available for measuring the surface roughness of the workpiece.

Machining parameters have significant and unique effects on each or all of the aforementioned process parameters. Machining parameters include the following:

1. Pulse-on time
2. Pulse-off time
3. Spark gap
4. Duty cycle
5. Polarity

A description of each of these machining parameters is presented below.

2.8.4 Pulse-on time

Pulse-on time (t_{on}) is the time period the current is allowed to flow through the electrode towards the work material within the spark gap. Metal removal is directly proportional to the amount of energy applied during the on-time period [32]. Material removal rate depends on pulse-on time periods. Longer pulse duration improves removal rate of debris from the machined area which also effects on the wear behavior of electrode. Because in EDM process erosion takes place in the form of melting and vaporization of both the tool and work material at the same time period, with longer pulse duration, more material has to melt and vaporize. The resulting crater produced will be broader in comparison to that at shorter pulse on time. However, in some experimental research work it has been reported there exists an optimal pulse duration that yields high performance measures [33]. It has been shown that MRR can not be increased by increasing the pulse-on time only; a suitable setting of peak current is also needed for increasing the MRR.

2.8.5 Pulse-Off time

Pulse-Off time(t_{0ff}) is the waiting interval between two pulses. It is the duration of time in which no machining takes place (idle time period) and it allows the melt material to vaporize. This parameter affects the speed and the stability of the cut. If this time period is short, it gives high MRR but it will cause more sparks to be unstable in the machining zone. Kansal *et al.* [34] showed that increase in pulse interval time decreases the MRR. Saha *et al.* [35] reported that for small values of pulse interval time period, the MRR was low, but with further increase MRR increases. MRR reduces slowly with increase in pulse interval time. This is due to the fact that with very short pulse interval the probability of arcing is larger because dielectric in the gap does not recover its dielectric strength. Abu Zeid investigated the role of voltage, pulse off time in the electro discharge machined AISI T1 high speed steel [36]. The researcher concluded that the MRR is not so much sensitive to pulse interval time changes at low pulse on time in finish machining.

2.8.6 Spark gap

This is the distance between the electrode and the workpiece during the process of EDM. Electro-mechanical and hydraulic systems are used to respond to average gap voltage. To obtain good performance and gap stability, a suitable gap should be maintained. For the reaction speed, it must obtain a high speed so that it can respond to short circuits or even open gap circuits. Gap width is not measured directly, but can be inferred from the average gap voltage [37].

2.8.7 Duty cycle

This is a percentage of the on-time relative to the total cycle time. This parameter is calculated by dividing the on-time by the total cycle time (on-time plus off-time). It indicates the degree

of efficiency of the operation.

$$Dutycycle = \frac{T_{on}}{T_{on} + T_{off}} \tag{2.16}$$

Amarim [38] studied the effect of duty cycle on MRR, and reported that increase in duty factor increases MRR. Krishna *et al.* [39] reported that MRR increases with increase in duty factor at constant current and constant pulse-on time. He attributed this to the fact that with increase in duty cycle, the intensity of spark increases resulting in higher MRR.

2.8.8 Polarity

This may be positive or negative connected to tool electrode or work material. Polarity can affect processing speed, finish, wear and stability of the EDM operation. It has been shown that MRR is more when the tool electrodes are connected at positive polarity(+) than at negative terminal(-). This is due to transfer of more energy during the charging process. When a electrical discharge is generated electrons dispatch from the negative polarity collides with neutral molecules between the work piece and electrode which is responsible for ionization process in EDM. However, ionization is taken because the electron arrives at the positive terminal of the surface. The negative polarity is more desirable as compared to positive polarity [20]. This is because the MRR is higher and better surface finish is produced as MRR is dependent on anode potential drop. Chow et al. carried out work on the micro slitting on titanium alloy with copper using a rotating disk as a electrode. He concluded that MRR was lower with positive polarity of work piece as compared to negative polarity. This is due to the fact that with positive polarity of work piece, the dissociated carbon elements in the dielectric fluid tend to adhere to the anode, which result in forming a recast layer [40].

Therefore, the selected settings of any particular machining parameter (duty cycle, pulse-on and off time and polarity) has a significant effect on the material removal rates, the surface roughness and the tool life. In this research a new machining parameter, magnetic intensity, is introduced and its effect on the process parameters investigated.

Chapter 3

METHODOLOGY

3.1 Experimental setup

The experiments and measurements in this research were undertaken at Diemould Machinery Product and Services Industry (DPMS) and at the National Youth Services (NYS) mechanical workshop. Experiments were carried out on a ToolCraft A25 sinker electrical discharge machine, Figure 3.1, fitted with a custom fabricated attachment for facilitating the introduction of the magnetic energy around the spark gap region.

Figure 3.1: Electric discharge machine

In order to establish the external magnetic field around the tool-workpiece system, pairs of magnets of intensity ranging between 1600G and 5903G was attached on either sides of the custom designed fixture. A specific fixed distance was maintained between the magnetic poles

for all sets of experiments. The properties of the magnets used in this research are outlined in Table 3.1.

Table 3.1: Magnet properties

Magnet	Pull-force(N)	Brmax(G)	BHmax(MGOe)
DY04	197.00	13200	42
DY08	467.06	13200	42
DY08n	578.26	14800	52
DY0X0	925.23	13200	42
DY0Y0	1356.70	13200	42

Figure 3.2 depicts the schematic diagram of the experimental setup. Here, magnets are located adjacent to the spark gap region at a fixed length.

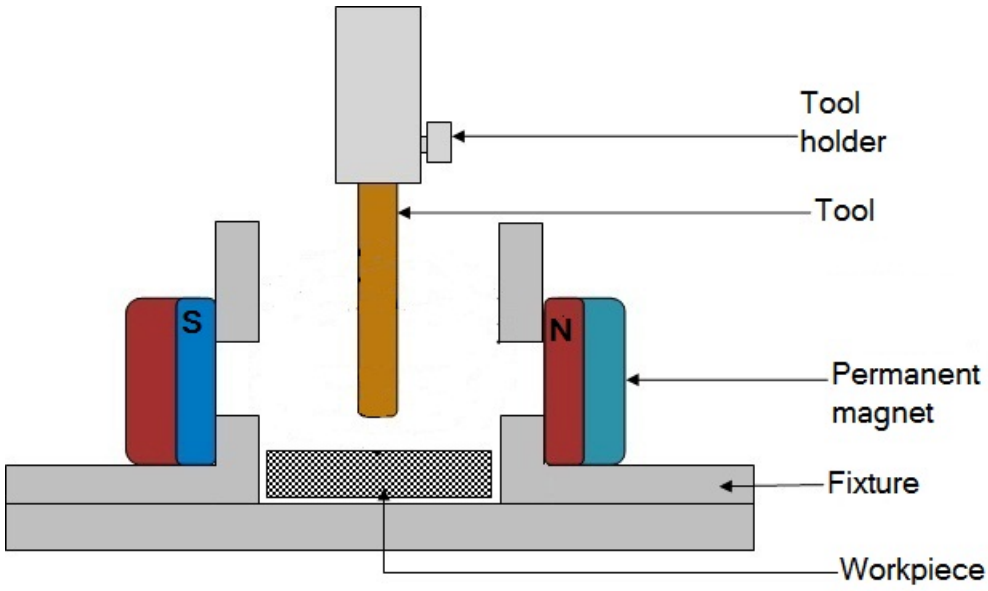

Figure 3.2: Schematic diagram of the experimental setup

The spark generator allowed for the variation and setting of various parameters including the pulse timing, current, pulse selection, auto arc and flushing setting. The outputs directly read from the machine included the average discharge current and voltage.

Figure 3.3 shows the machining setup before the tank is filled with dielectric fluid. The tool holder and the copper electrode are also shown.

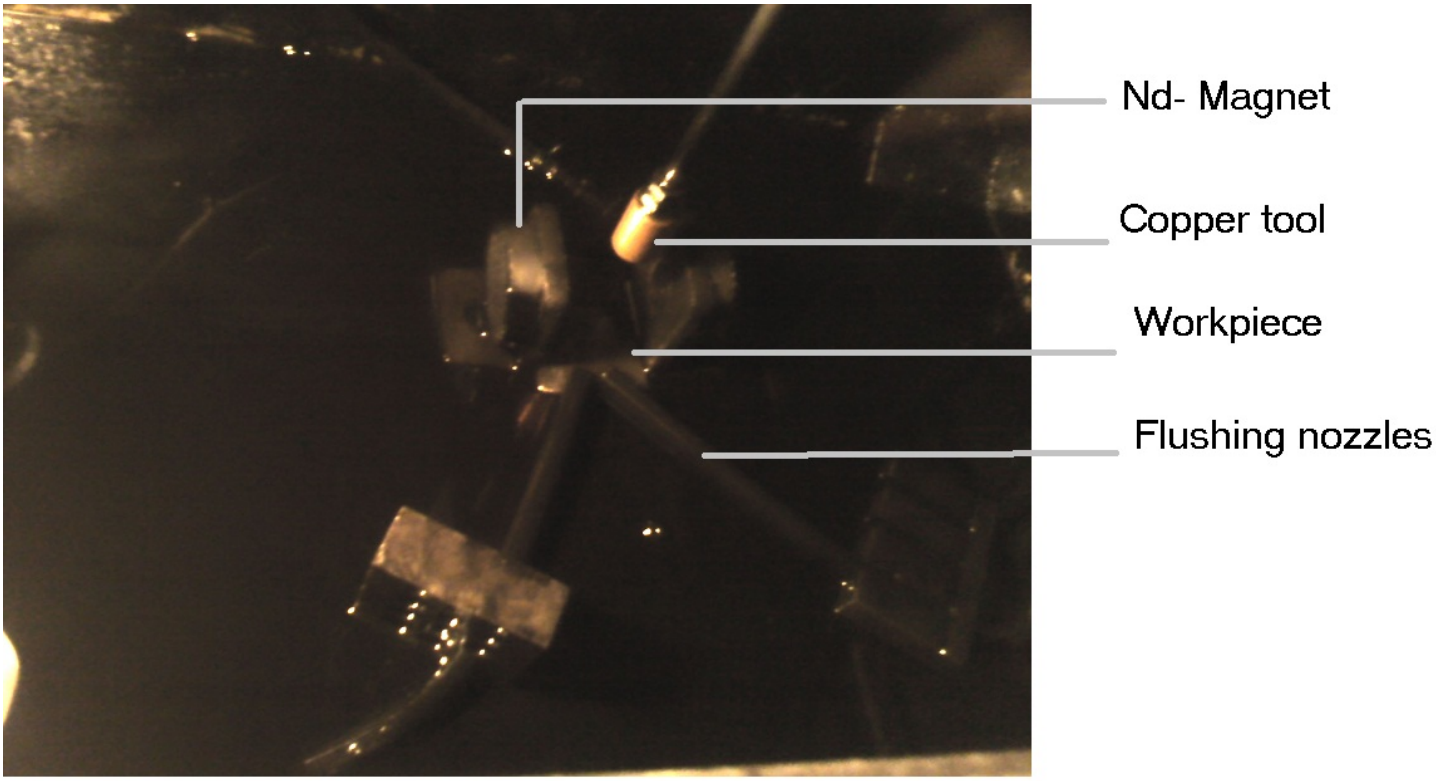

Figure 3.3: Actual experimental setup

3.2 Experimental materials

The workpiece material was mild steel while the tool material was copper. The dimension of the workpiece specimen was 50mm by 50mm by 5mm. The surface of workpiece specimen was milled and ground to ensure parallelism and surface roughness uniformity before conducting the experiment.

The tool-electrode's front face was machined to a diameter of 25mm and overall length cut to 35mm. The end face of the electrode against the workpiece was ground using emery cloth. These design dimensions were selected based on availability of the materials and ease of ma-

chining. In addition, kerosene was used as the dielectric fluid in this investigation.

3.3 Experimental procedure

After configuring the experimental setup, experiments on the effect of various levels of magnetic strength, pulse-off time, discharge current and pulse-on time on EDM machining parameters was conducted.

The machining parameters used in this study are given in Table 3.2.

Table 3.2: Machining parameters

Parameter	**Value**
Magnetic intesity	1601 - 5903 G
Current (I)	3.125 - 23.4375 A
Pulse-on time(T_{on})	50 - 90 μs
Pulse-off time(T_{off})	50 - 90 μs
Tool electrode diameter	25 mm
Tool electrode material	copper
Work-piece material	Mild steel
Dielectric fluid	kerosene

On each experimental run the workpiece and electrode specimens were weighed using an electronic balance before and after each experiment to calculate MRR and TWR. The machining time was set at 4 min for each machining condition. Material removal rate and tool wear rate in this experiments were obtained by dividing the weight difference of the workpiece/tool - before and after machining - with the time taken to machine it.

After machining, the surface roughness of the surface generated was measured. A mitutoyo surftest-402, Figure3.4, was used to evaluate the surface quality of the machined surface. This was done at the National Youth Service (NYS) mechanical workshop.

Confirmation readings were done using precision Phase II SRG-4000, portable surface roughness tester.

Figure 3.4: Surface roughness measurement

3.4 Design of experiment and Modelling

The theoretical background expounding on the design of experiment is outlined in Appendix A and details can be obtained in ref [49]. The levels of the pertinent process parameters selected for the present investigation were chosen as -2, -1, 0, 1, 2 in coded form to have a rotatable design. Table 3.3 shows the factors and their levels in coded and actual values.

Table 3.3: Factor levels

Parameter	**Symbol**	**-2**	**-1**	**0**	**1**	**2**
Magnetic intensity,G	M	1601	2952	3309	4667	5903
Pulse-on time,μs	T_n	50	60	70	80	90
Current,A	I	3.125	9.375	15.625	21.875	23.4375
Pulse-off time,μs	T_{off}	50	60	70	80	90

For the four variables, the design required 31 experiments with 16 factorial points (2^4); 8 ax-

ial points form a central composite design with α=2, and 7 centre points for replication to estimate the experimental error. The design was generated and analysed using the MINITAB statistical package.

Models were developed from the experimental data showing the relationship and expected outcomes of variation of the machining parameters. The modelling was approached empirically in line with most research studies carried out in the field of EDM . Response surface method was employed in the development of the model and analysis of the research variables. The focus was on establishing the relationship between the dependent variables (MRR, TWR and Surface finish) and the independent variable (magnetic intensity, pulse-on time,peak current and pulse-off time).

Response surface method was employed to determine the operating conditions that produce the best response and to model a relationship between the quantitative factors and the response.

The modelling was carried out in the following steps:

(a) Identifying the process control variables of interest and finding their upper and lower limits.

(b) Developing the design matrix.

(c) Conducting the experiments as per the design matrix.

(d) Recording the response parameters.

(e) Developing quadratic models and calculating the regression coefficients.

(f) Checking the adequacy of models.

(g) Testing the significance of coefficients and arriving at the final models.

(h) Illustrating the direct and interaction effects graphical form.

(i) Analysis of results.

Figure 3.5 shows the CCD and the randomized experimental runs in coded form.

Central Composite Design

Factors:	4	Replicates:	1
Base runs:	31	Total runs:	31
Base blocks:	1	Total blocks:	1

Two-level factorial: Full factorial

Cube points:	16
Center points in cube:	7
Axial points:	8
Center points in axial:	0

Alpha: 2

Design Table (randomized)

Run	Blk	A	B	C	D
1	1	1	-1	1	1
2	1	-1	1	1	1
3	1	-1	1	-1	-1
4	1	1	-1	-1	-1
5	1	-1	-1	-1	-1
6	1	-1	1	1	-1
7	1	-1	-1	1	1
8	1	0	0	0	0
9	1	0	0	0	-2
10	1	2	0	0	0
11	1	0	0	0	0
12	1	-1	-1	-1	1
13	1	1	-1	1	-1
14	1	-1	-1	1	-1
15	1	0	-2	0	0
16	1	1	1	1	-1
17	1	0	0	0	0
18	1	-2	0	0	0
19	1	1	1	-1	-1
20	1	0	0	0	0
21	1	0	0	0	2
22	1	0	0	0	0
23	1	1	1	-1	1
24	1	1	1	1	1
25	1	0	0	0	0
26	1	0	2	0	0
27	1	0	0	0	0
28	1	1	-1	-1	1
29	1	0	0	-2	0
30	1	0	0	2	0
31	1	-1	1	-1	1

Figure 3.5: Central composite design summary

The response surface method is a sequential process and in this research, it was executed using the procedure summarized as shown in Figure 3.6.

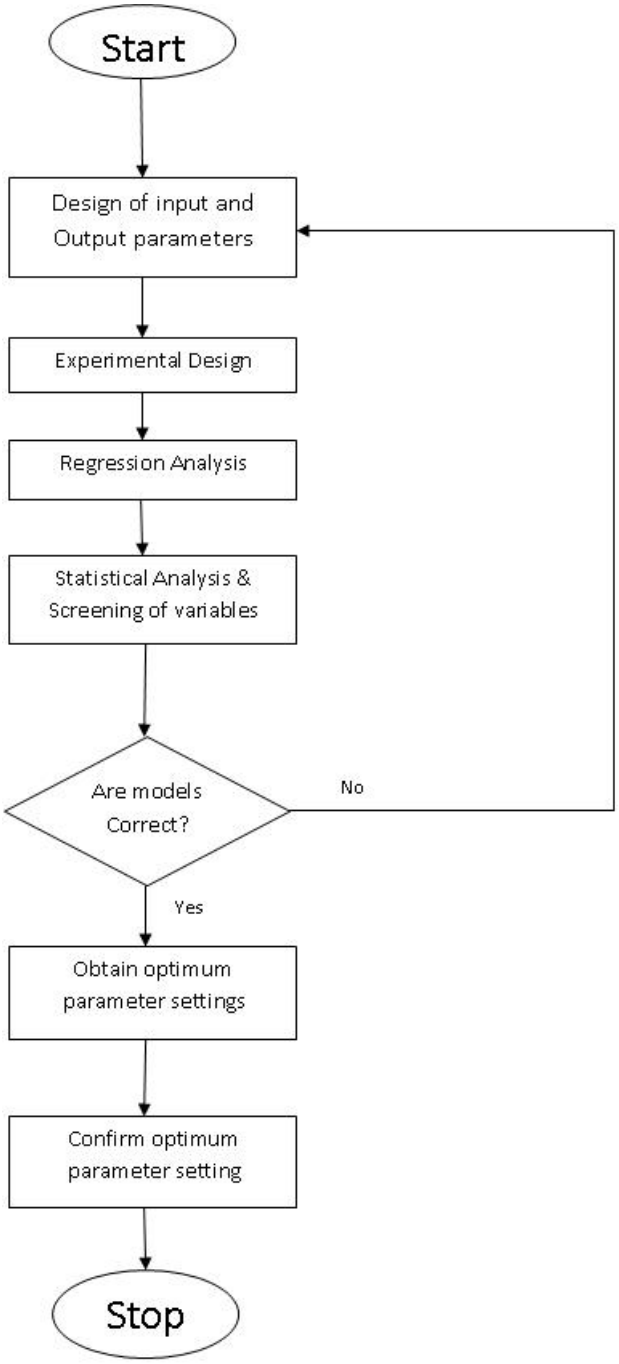

Figure 3.6: Execution procedure for RSM

Chapter 4

RESULTS AND DISCUSSION

4.1 Results and models

4.1.1 Analysis and modelling

The EDM process was studied with a standard RSM design. MINITAB software was used for regression and graphical analysis of the data obtained. The optimum values of the selected variables were obtained by solving the regression equation and by analysing the response surface contour plot.

The experiments were conducted in duplicate following the selected CCD design (Appendix A). The resulting values of MRR, TWR and Ra are tabulated in Table B.1. Comparison with results obtained from experimental runs with jet flushing only (Appendix B) confirmed that the introduction of magnetic intensity had significant effects on the parameters.

Before data analysis, it was necessary to check whether the model was a good fit. This involved testing for significance of the regression model, significance of model coefficients and for lack of fit. For this purpose, analysis of variance (ANOVA) was performed.

Table 4.1: Experimental results

Expt No.	M(G)	$T_n(\mu s)$	I(A)	$T_{off}(\mu s)$	MRR(mg/min)	TWR(mg/min)	Ra(μm)
1.	4667	60	21.875	80	270.00	15.32	9.429
2.	1601	80	21.875	80	365.33	13.33	11.17
3.	1601	80	9.375	60	260.00	15.67	8.5
4.	4667	60	9.375	60	240.67	16.09	8.3
5.	2952	60	9.375	60	206.67	16.37	7.0
6.	2952	80	21.875	60	267.33	15.61	9.5
7.	2952	60	21.875	80	316.67	14.67	8.5
8.	3309	70	15.625	60	280.00	15.01	11.61
9.	3309	70	15.625	50	290.93	14.92	3.2
10.	5903	70	15.625	70	285.33	14.99	11.97
11.	3309	70	15.625	70	280.00	15.01	11.61
12.	2952	60	9.375	80	249.97	15.97	10.21
13.	4667	60	21.875	60	260.97	15.60	7.7
14.	2952	60	21.875	60	260.33	15.63	11.3
15.	3309	50	15.625	70	256.67	16.09	10.0
16.	4667	80	21.875	60	230.33	16.76	10.01
17.	3309	70	15.625	70	280.00	15.01	11.61
18.	1601	70	15.625	70	260.67	15.68	11.97
19.	4667	80	9.375	60	200.00	16.97	9.7
20.	3309	70	15.625	70	280.00	15.01	11.61
21.	3309	70	15.625	90	333.33	14.01	10.5
22.	3309	70	15.625	70	295.67	24.19	12.21
23.	4667	80	9.375	80	363.33	13.67	11.2
24.	4667	80	21.875	80	386.67	13.25	13.72
25.	3309	70	15.625	70	295.67	13.87	12.21
26.	3309	90	15.625	70	226.67	16.83	12.70
27.	3309	70	15.625	70	280.0	15.05	11.61
28.	4667	60	9.375	80	255.6	16.11	10.21
29.	3309	70	3.125	70	320.00	14.33	8.5
30.	3309	70	23.4375	70	350.00	13.67	11.72
31.	2952	80	9.375	80	370.00	13.33	13.12
32.	5903	60	9.375	60	251.09	15.99	8.90
33.	3309	60	9.375	60	224.32	16.23	7.60
34.	1601	60	9.375	60	201.53	16.44	6.3

4.1.2 Model for material removal rate

The modelling for the material removal rate (MRR) was carried out using RSM. The fit summary recommended that the quadratic model is statistically significant for analysis of MRR. This is indicated by a P-value of 0 for the lack-of-fit check. The ANOVA table for the quadratic model for MRR is shown in Table 4.2. The P-value for the linear terms indicate that these are more significant as compared to the square and interaction terms which have lower confidence levels.

Table 4.2: ANOVA table for MRR

Source.	**DF**	**seq SS**	**adj SS**	**adj MS**	**F**	**P**
Regression	14	51647.9	51647.9	3689.1	3.88	0.006
Linear	4	30031.6	30031.6	7507.9	7.89	0.001
M	1	64.7	64.7	64.7	0.07	0.798
$\mathbf{T}_n$	1	4323.1	4323.1	4323.1	4.54	0.049
I	1	3068.9	3068.9	3068.9	3.23	0.091
$\mathbf{T}_{off}$	1	22575.0	22575.0	22575.0	23.73	0.00
Square	4	10277.4	10277.4	2569.4	2.70	0.068
M$\times$ **M**	1	662.4	544.2	544.2	0.57	0.460
$\mathbf{T}_n\times\ \mathbf{T}_n$	1	5549.0	4252.6	4252.6	4.47	0.051
I$\times$ **I**	1	3226.0	3547.3	3547.3	3.73	0.071
$\mathbf{T}_{off}\times\ \mathbf{T}_{off}$	1	840.1	840.1	840.1	0.88	0.361
Interaction	6	11338.9	11338.9	1889.	1.99	0.128
M$\times\ \mathbf{T}_n$	1	360.3	360.3	360.3	0.38	0.547
M$\times$ **I**	1	75.0	75.0	75.0	0.08	0.782
M$\times\ \mathbf{T}_{off}$	1	81.0	81.0	81.0	0.09	0.774
$\mathbf{T}_n\times$ **I**	1	609.2	609.2	609.2	0.64	0.435
$\mathbf{T}_n\times\ \mathbf{T}_{off}$	1	10204.5	10204.5	10204.5	10.73	0.005
I$\times\ \mathbf{T}_{off}$	1	8.8	8.8	8.8	0.01	0.925
Residual error	16	15221.8	15221.8	951.4		
Lack-of-fit	10	14871.1	14871.1	14871.1	25.44	0.000
Pure error	6	350.8	350.8	58.5		
Total	30	66869.8				

The results of the quadratic model for MRR are given in Table 4.3. The value of R^2 is at 77.24 % indicating the regression model is providing a good representation of the relationship between the independent variables (factors) and the response (MRR).

Table 4.3: Regression coefficients for MRR

Term	Coefficient	T	P
Constant	284.477	24.402	0.000
M	-1.642	-0.261	0.798
T_n	13.421	2.132	0.049
I	11.308	1.796	0.091
T_{off}	30.670	4.871	0.000
M×M	-4.362	-0.756	0.460
$T_n \times T_n$	-12.195	-2.114	0.051
I×C	11.138	1.931	0.071
$T_{off} \times T_{off}$	5.420	0.940	0.361
$M \times T_n$	-4.746	-0.615	0.547
M×C	-2.166	-0.281	0.782
$M \times T_{off}$	2.249	0.292	0.774
$T_n \times C$	-6.171	-0.800	0.435
$T_n \times T_{off}$	25.254	3.275	0.05
$I \times T_{off}$	-0.741	-0.096	0.925

S = 30.8442 PRESS = 86134.8

R-Sq = 77.24% R-Sq(adj) = 57.32%

The associated P-value for the model is lower than 0.05(i.e. taking α=0.05 or 95% confidence) indicating that the model is considered to be statistically significant. For a 90% confidence level, the linear effect of the factor T_n (95.1 %), I (90.9 %), T_{off} (100 %) are significant. The quadratic effect of the factor T_n and I together with the interaction effects of T_n and T_{off} are also significant.

The final response equation for MRR is given in equation 4.1

$$MRR = 284.477 - 1.642M + 13.421T_n + 11.308I + 30.670T_{off} - 4.362M^2$$
$$- 12.195T^2{}_n + 11.138I^2 + 5.420T^2{}_{off} - 4.746MT_n - 2.166MI \quad (4.1)$$
$$+ 2.249MT_{off} - 6.171T_nI + 25.254T_nT_{off} - 0.741IT_{off}$$

Where M is magnetic field intensity in Gauss, T_n is pulse-on time in micro-seconds, I is current in amperes and T_{off} is pulse-off time in micro-seconds.

A trend curve showing the relationship between MRR and magnetic intensity at constant duty cycle (T_n = 60 μ s, T_{off}= 60 μ s) and current (9.375 A) is shown in Figure 4.1. It is seen that material removal rate increases with increase in high magnetic intensity levels.

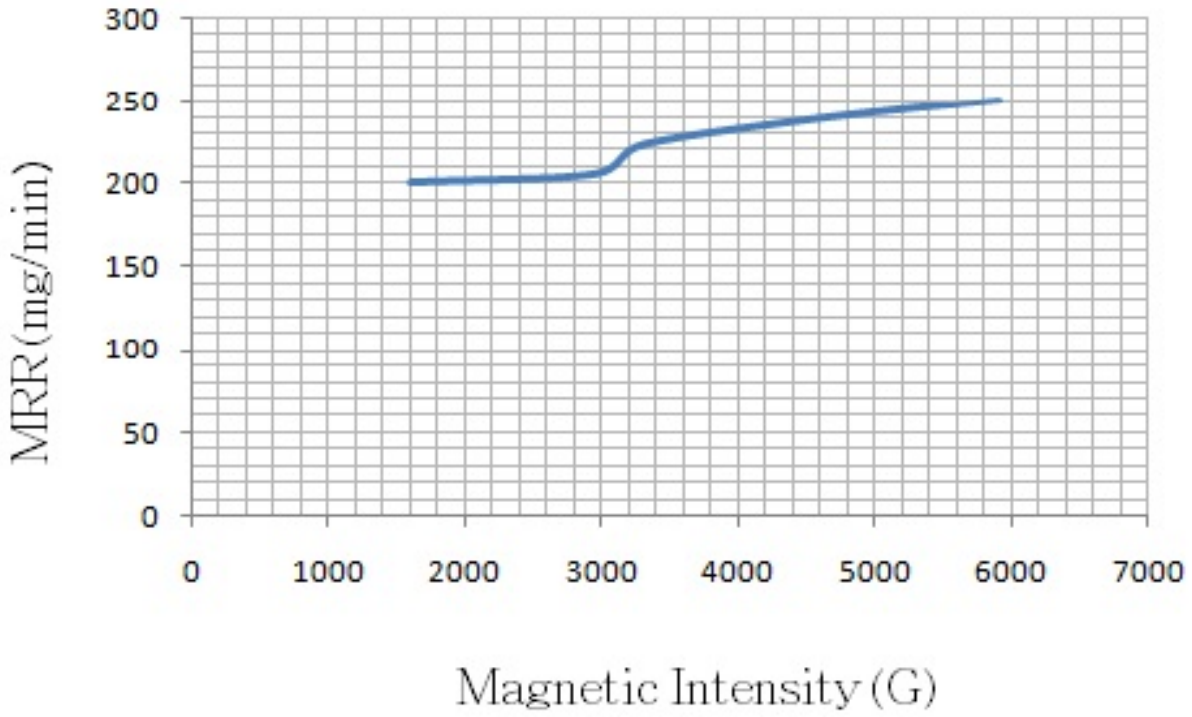

Figure 4.1: Influence of magnetic intensity on MRR

To check that the quadratic model for MRR fits appropriately, the normal probability graph of the residuals for MRR was plotted. This is shown in Figure 4.2. The residuals are falling on

a straight line which means that the errors are normally distributed and the regression model agrees well with the observed values.

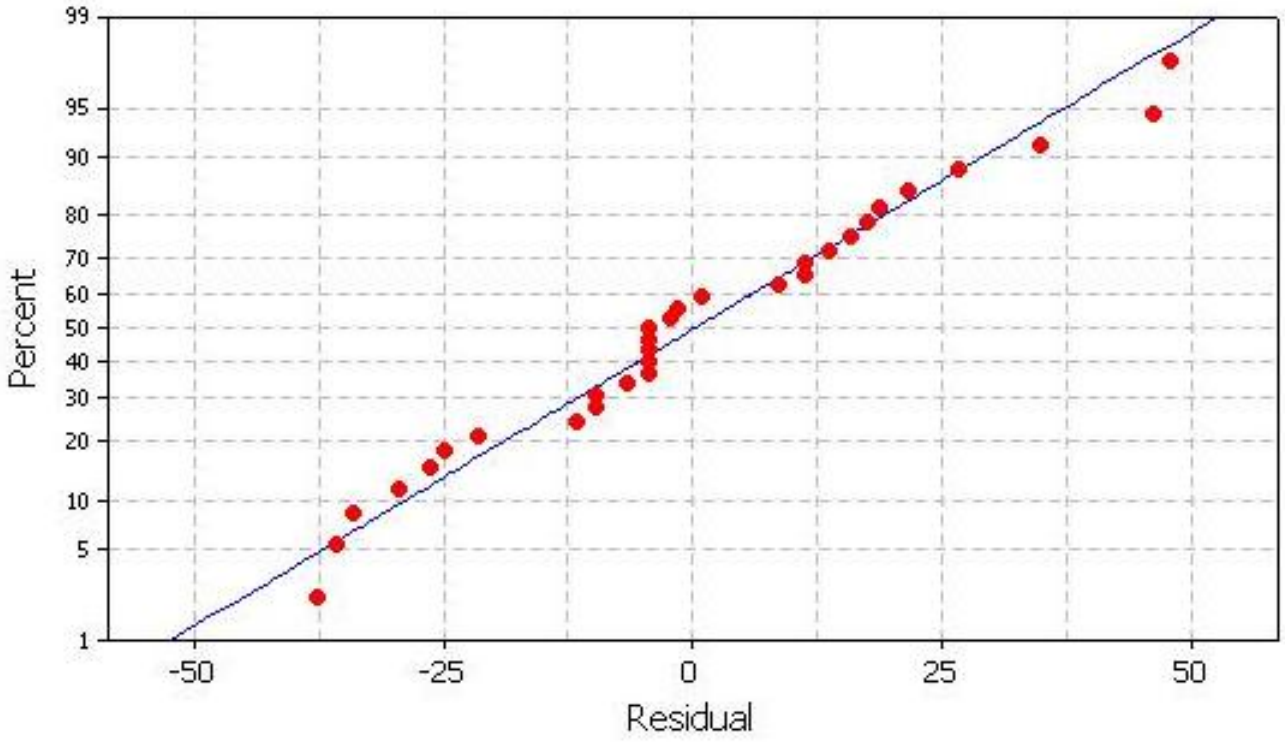

Figure 4.2: Normal probability plot residuals for MRR

4.1.3 Model for surface roughness

The ANOVA results for the quadratic model for the surface roughness (Ra) is shown in Table 4.4.

Table 4.4: ANOVA table for Ra

Source.	**DF**	**seq SS**	**adj SS**	**adj MS**	**F**	**P**
Regression	14	113.802	113.802	8.127	6.18	0.000
Linear	4	57.819	57.819	14.4547	10.98	0.000
M	1	0.039	0.039	0.0391	0.03	0.865
$\mathbf{T}_n$	1	16.123	16.123	16.1228	12.25	0.003
I	1	3.783	3.783	3.7834	2.87	0.109
$\mathbf{T}_{off}$	1	37.873	37.873	37.8734	28.77	0.000
Square	4	48.331	48.331	12.0829	9.18	0.000
MxM	1	1.056	0.027	0.0275	0.02	0.887
$\mathbf{T}_n\mathbf{xT}_n$	1	0.042	0.440	0.4398	0.33	0.571
IxI	1	2.623	5.387	5.3865	4.09	0.060
$\mathbf{T}_{off}\mathbf{xT}_{off}$	1	44.610	44.610	44.6103	33.89	0.000
Interaction	6	7.652	7.652	1.2753	0.97	0.477
$\mathbf{MxT}_n$	1	0.861	0.861	0.8607	0.65	0.431
MxI	1	0.002	0.002	0.0023	0.00	0.967
$\mathbf{MxT}_{off}$	1	0.289	0.289	0.2866	0.22	0.646
$\mathbf{T}_n\mathbf{xI}$	1	0.028	0.028	0.0281	0.02	0.886
$\mathbf{T}_n\mathbf{xT}_{off}$	1	3.470	3.470	3.4698	2.64	0.124
$\mathbf{IxT}_{off}$	1	3.002	3.002	3.0024	2.28	0.150
Residual error	16	21.062	21.062	1.3164		
Lack-of-fit	10	20.548	20.548	2.0548	23.97	0.000
Pure error	6	0.514	0.514	0.0857		
Total	30	134.864				

The linear and square factors were observed to be highly significant as compared to the interaction factors.

The results of the quadratic model for R_a are given in Table 4.5. The value of R^2 is 84.38% indicating that the regression model is providing an excellent representation of the relationship between the independent variables (factors) and the response (Ra).

Table 4.5: Regression coefficients for Ra

Term	Coefficient	T	P
Constant	11.7814	27.168	0.000
M	0.0404	0.172	0.865
T_n	0.8196	3.500	0.003
I	0.3970	1.695	0.109
T_{off}	1.2562	5.364	0.000
M×M	0.0310	0.144	0.887
$T_n \times T_n$	-0.1240	-0.578	0.571
I×I	-0.430	-2.023	0.060
$T_{off} \times T_{off}$	-1.2490	-5.821	0.000
$M \times T_n$	0.2319	0.809	0.431
M×I	-0.0119	-0.042	0.967
$M \times T_{off}$	0.1343	0.468	0.646
$T_n \times I$	0.0419	0.146	0.886
$T_n \times T_{off}$	0.4657	1.624	0.124
$I \times T_{off}$	-0.4332	-1.510	0.150

S = 1.14734 PRESS = 119.056

R-Sq = 84.38% R-Sq(adj) = 70.72%

For a 95% significance level, the linear factors T_n and T_{off} are applicable. This is also true for the square factor T_{off}.

The response equation for Ra is given in equation 4.2

$$\begin{aligned} R_a = {} & 11.7814 + 0.0404M + 0.8196T_n + 0.3970I + 1.2562T_{off} + 0.0310M^2 \\ & - 0.1240{T^2}_n - 0.430I^2 - 1.2490{T^2}_{off} + 0.2319MT_n - 0.0119MI \\ & + 0.1343MT_{off} + 0.0419IT_n + 0.4657T_nT_{off} - 0.4332IT_{off} \end{aligned} \tag{4.2}$$

M is the magnetic field intensity in Gauss, T_n is pulse-on time in micro-seconds, I is current in amperes and T_{off} is pulse-off time in micro-seconds.

Figure 4.3, shows the relationship between Ra and magnetic intensity at constant duty cycle and current. It is seen that the surface roughness of a workpiece machined in the presence of a magnetic field increases with increase in the magnetic intensity.

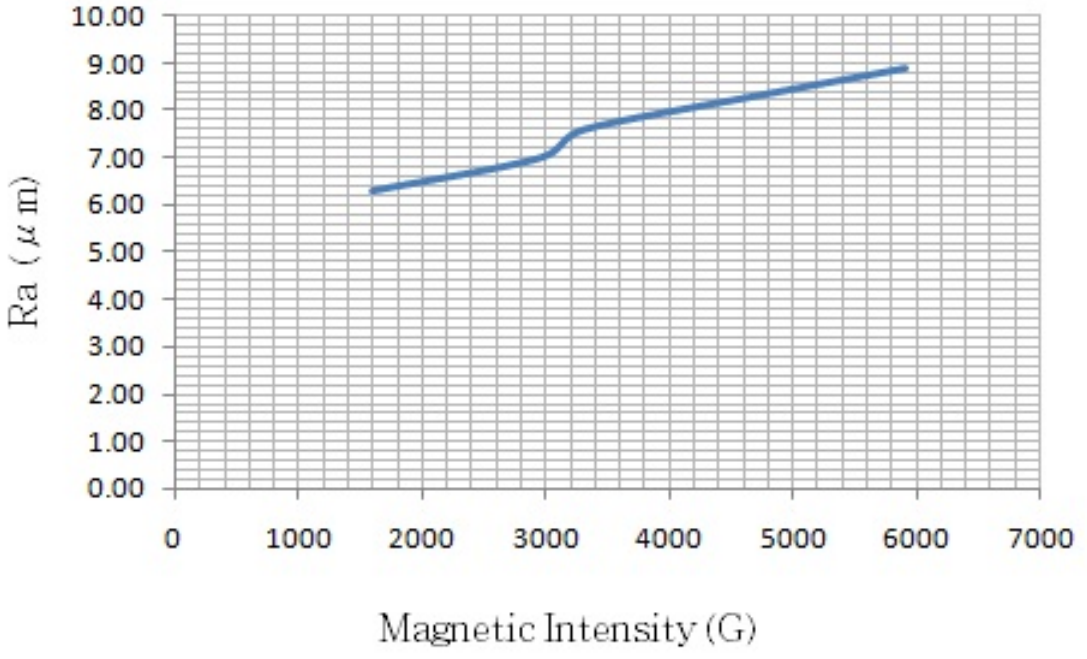

Figure 4.3: Influence of magnetic intensity on Ra

To ascertain proper fitting of the quadratic model for Ra, the normal probability graph of the

residuals for Ra was plotted as shown in Figure 4.4. The residuals are falling on a straight line which means that the errors are normally distributed and the regression model agrees fairly well with the observed values.

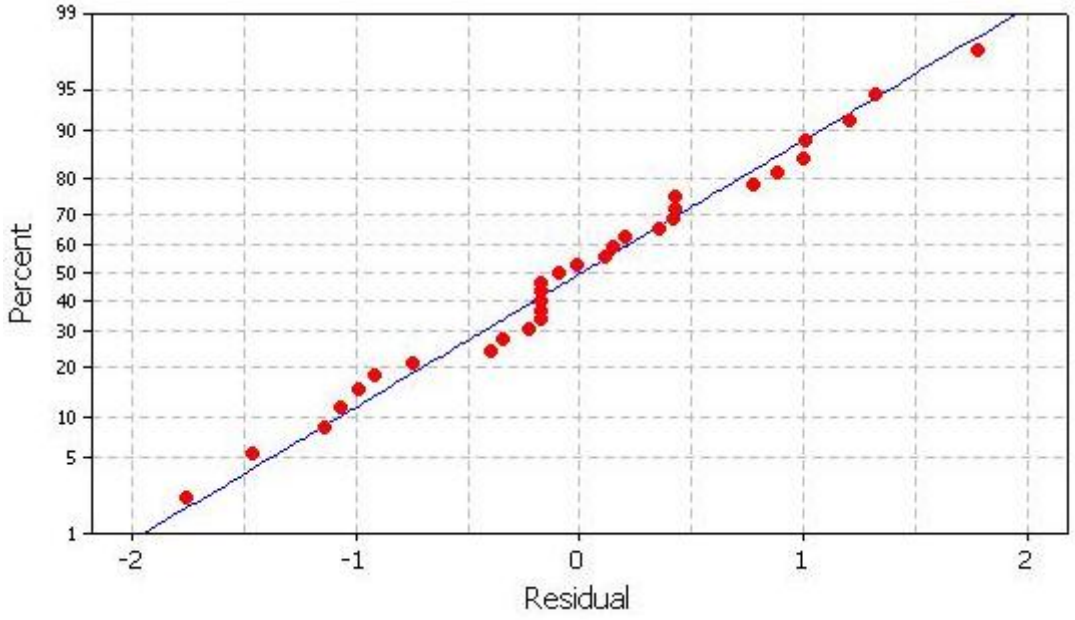

Figure 4.4: Normal probability plot residuals for R_a

4.1.4 Model for tool wear rate

The ANOVA results for the quadratic model for the tool wear rate (TWR) is shown in Table 4.6.

The P-value for the model is at a 95% confidence level indicating that the model is considered statistically significant.

Table 4.6: ANOVA table for TWR

Source.	**DF**	**seq SS**	**adj SS**	**adj MS**	**F**	**P**
Regression	14	25.8711	25.8711	1.84973	2.81	0.025
Linear	4	11.8960	11.8960	2.97401	4.53	0.012
M	1	0.1380	0.1380	0.13802	0.21	0.653
$\mathbf{T}_n$	1	1.3443	1.3443	1.34427	2.05	0.172
I	1	1.1882	1.1882	1.18815	1.81	0.197
$\mathbf{T}_{off}$	1	9.2256	9.2256	9.22560	14.04	0.002
Square	4	7.0652	7.0652	1.76631	2.69	0.069
MxM	1	0.2332	0.2249	0.22493	0.34	0.567
$\mathbf{T}_n\mathbf{xT}_n$	1	4.8094	3.9135	3.19350	5.96	0.027
IxI	1	1.5841	1.7173	1.71729	2.61	0.125
$\mathbf{T}_{off}\mathbf{xT}_{off}$	1	0.4745	0.4745	0.47446	0.72	0.408
Interaction	6	6.9098	6.9098	1.15163	1.75	0.173
$\mathbf{MxT}_n$	1	0.3136	0.3136	0.31360	0.48	0.500
MxI	1	0.002	0.002	0.0023	0.00	0.967
$\mathbf{MxT}_{off}$	1	0.0756	0.0756	0.07563	0.12	0.739
$\mathbf{T}_n\mathbf{xI}$	1	0.4290	0.4290	0.42903	0.65	0.431
$\mathbf{T}_n\mathbf{xT}_{off}$	1	6.0270	6.0270	6.02703	9.17	0.008
$\mathbf{IxT}_{off}$	1	0.0625	0.0625	0.06250	0.10	0.762
Residual error	16	10.5121	10.5121	0.65701		
Lack-of-fit	10	5.8338	5.8338	0.58338	0.75	0.004
Pure error	6	4.6783	4.6783	0.77971		
Total	30	36.3832				

The results of the quadratic model for TWR are given in Table 4.7.

The value of R^2 is at 71.11% indicating that the regression model provides a good representation of the relationship between the independent variables (factors) and the response (TWR).

Table 4.7: Regression coefficients for TWR

Term	Coefficient	T	P
Constant	15.1186	49.349	0.000
M	0.0758	0.458	0.653
T_n	-0.2367	-1.430	0.172
I	-0.2225	-1.345	0.197
T_{off}	-0.6200	-3.747	0.002
M×M	0.0887	0.585	0.567
$T_n \times T_n$	0.3699	2.441	0.027
I×I	-0.2451	-1.617	0.125
$T_{off} \times T_{off}$	-1.1288	-0.850	0.408
$M \times T_n$	0.1400	0.691	0.500
M×I	0.0113	0.056	0.956
$M \times T_{off}$	-0.0688	-0.0339	0.739
$T_n \times I$	0.1638	0.808	0.431
$T_n \times T_{off}$	-0.6138	-3.029	0.008
$I \times T_{off}$	-0.0625	-0.308	0.762

S = 0.810559 PRESS = 39.9704

R-Sq = 71.11% R-Sq(adj) = 45.83%

The linear factor T_{off} is seen to be highly significant. Square factor T_{off} and interaction factors T_n and T_{off} are also observed to be highly significant with over 95% confidence levels. The response equation for TWR is given in equation 4.3

$$\begin{aligned} TWR = {} & 15.1186 + 0.0758M - 0.2367T_n - 0.2225I - 0.6200T_{off} + 0.0887M^2 \\ & + 0.3699{T^2}_n - 0.2451I^2 - 1.1288{T^2}_{off} + 0.1400MT_n + 0.0113MI \\ & - 0.0688MT_{off} + 0.1638T_nI - 0.6138T_nT_{off} - 0.0625IT_{off} \end{aligned} \tag{4.3}$$

M being magnetic field intensity,T_n being pulse-on time, I current and T_{off} being pulse-off time. Figure 4.5, which shows the relationship between TWR and magnetic intensity at constant duty cycle and current, indicates that the tool wear rate reduces with increase in magnetic intensity.

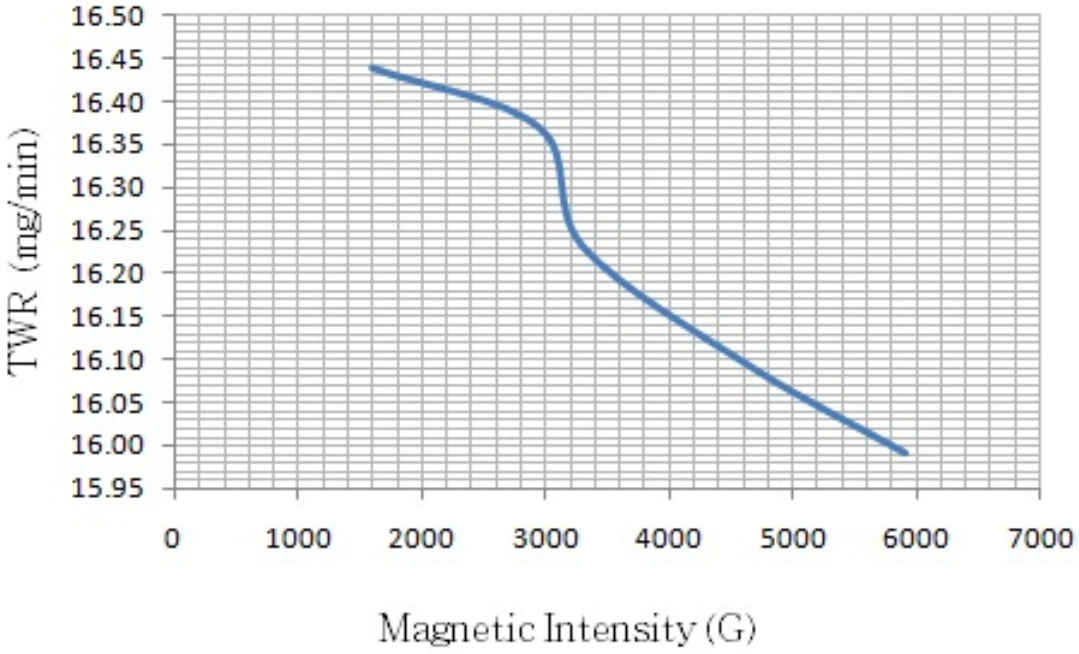

Figure 4.5: Influence of magnetic intensity on TWR

To fit the quadratic model for TWR appropriately Figure 4.6 displays the normal probability plot of the residuals for TWR. The residuals falling on a straight line which means that the errors are normally distributed and the regression model agrees fairly well with the observed values.

4.2 Response analysis

The effects of parameters on MRR, Ra and TWR were analysed through contour and surface plots. These plots enabled the response to be visualized and the selection of optimum settings for desired response outcomes. Statistical optimization was also carried out and the results compared with the response plots.

In machining, interaction between the parameters plays an important role. An interaction occurs when the change in response from one level of a factor to another level differs from the

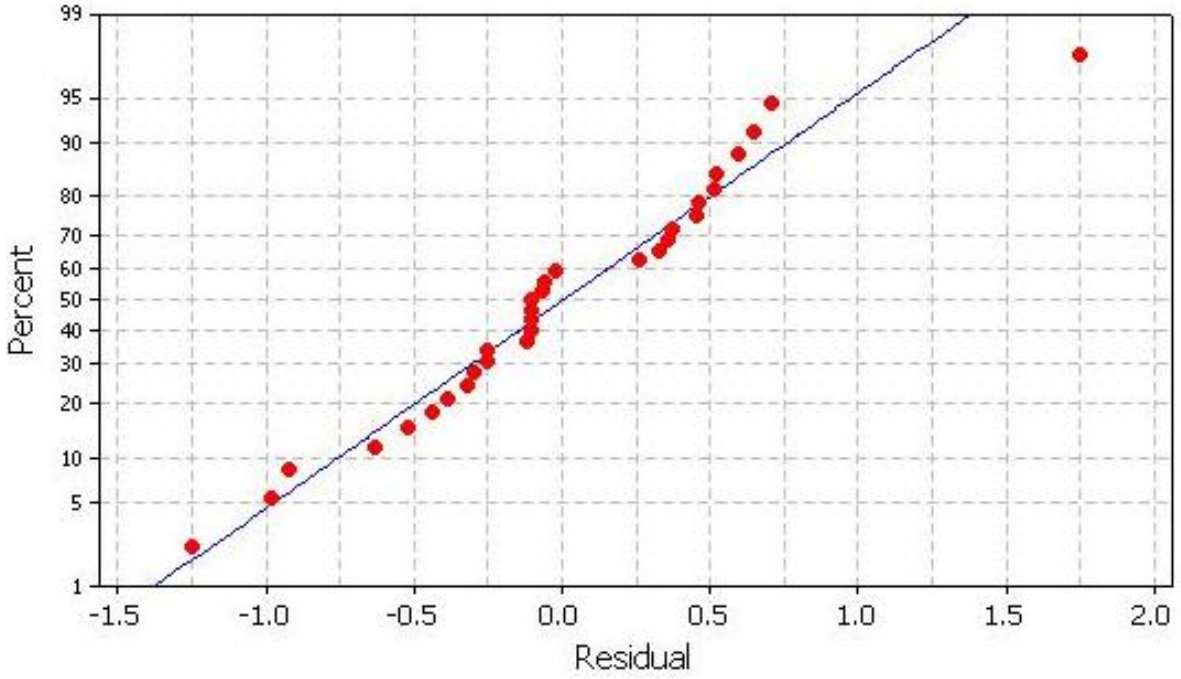

Figure 4.6: Normal probability plot residuals for TWR

change in response at the same two levels of a second factor. That is, the effect of one factor is dependent upon a second factor.

For a thourough response analysis, three levels of hold values were selected. These are oulined in Table 4.8 below. This allowed sufficient investigation of all interactions.

Table 4.8: Hold values

Factor	**High**	**medium**	**low**
M(G)	5903	3309	1601
$T_n(\mu s)$	9	7	5
I(A)	23.44	15.63	3.125
$T_{off}(\mu s)$	9	7	5

4.2.1 MRR response analysis

Table 4.9 shows the factors interactions considered for MRR and their confidence levels.

Table 4.9: Interactions and confidencle levels

Interaction	**Confidence level**
T_n - M	14
T_{off} - M	10.8
I - M	50
T_{off} - T_n	59.5
I - T_n	99.7
I - T_{off}	8

It is observed that the current(I) and pulse-on time(T_n) are highly dependent on each other at 99.7% . On the other hand, current and pulse-off time are least dependent on each other.

Figure 4.7 shows the response surface for MRR in relation to the design parameters of magnetic intensity (M) and pulse-on time (T_n). At high hold values, the MRR tends to increase considerably with increase in pulse-on time. High MRR values ($\geq$425 mg/min) are obtained at magnetic field intensity of between 4000G - 6000G and pulse-on time of around 85 μs. At medium levels, Figure 4.7b, high MRR values($\geq$280 mg/min) are observed at pulse-on time levels of between 70μs and 80μs and magnetic field intensity of between 2000G and 5000G.

At low hold levels,4.7c, high MRR values ($\geq$275 mg/min) are observed at pulse-on time levels lower than 70μs and magnetic field intensity levels below 4200G.

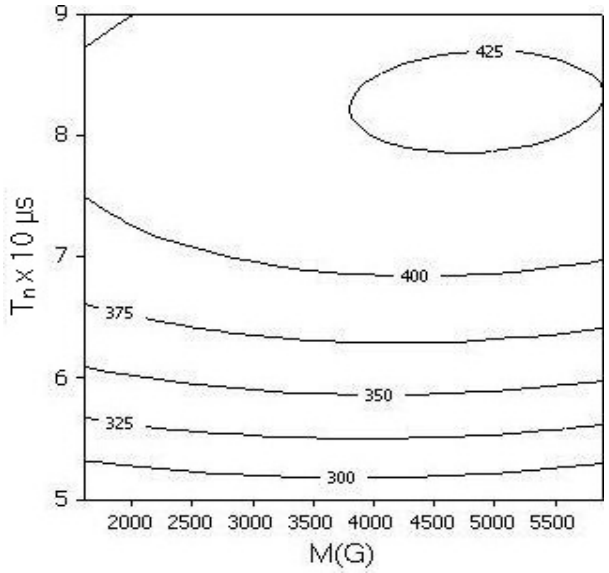

(a) High hold values

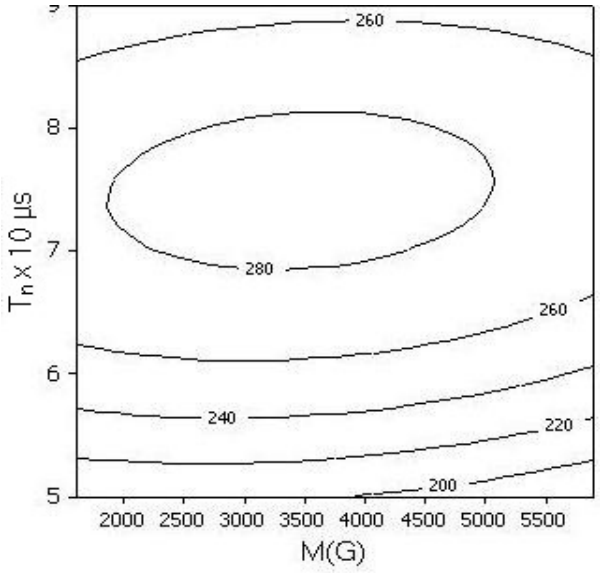

(b) medium hold values

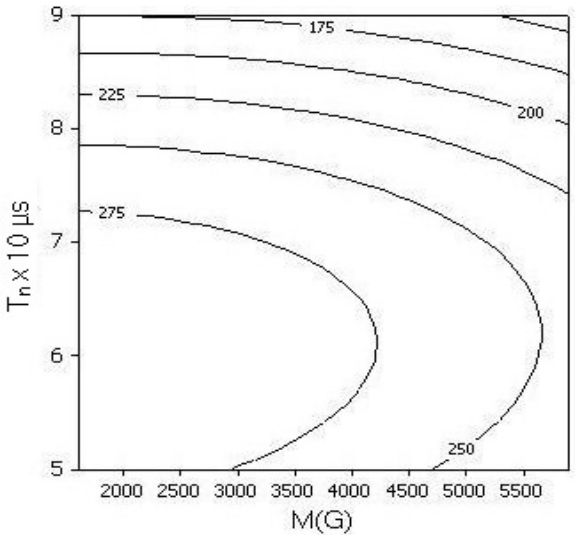

(c) low hold values

Figure 4.7: Response Plot of MRR vs T_n, M

It is concluded from the above results that with regards to magnetic intensity and pulse-on time levels, the settings providing the highest levels of MRR (the maximum material removal rates) are at maximum hold values (T_{off}=9μs,I=23.44A) and M$\geq$4000G, Tn$\geq$80μs.

The interaction effect of Pulse-off time (T_{off}) and Magnetic intensity (M) on MRR is shown in Figure 4.8. At high hold setting, the value of MRR is highest($\geq$435mg/min) when the magnetic intensity is at its upper values(5500G) and the pulse-off time is at its lowest($\leq$55 μs). At medium setting, MRR is seen to be more influenced by pulse-off time with the highest values($\geq$340mg/min) being recorded at T_{off} values above 90μs.

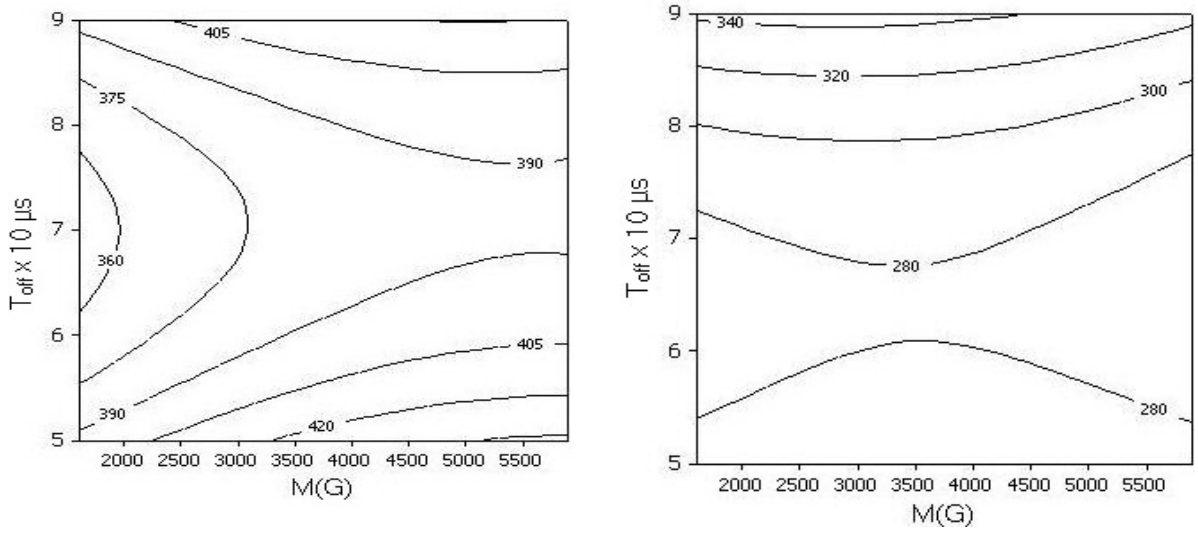

(a) High hold values

(b) medium hold values

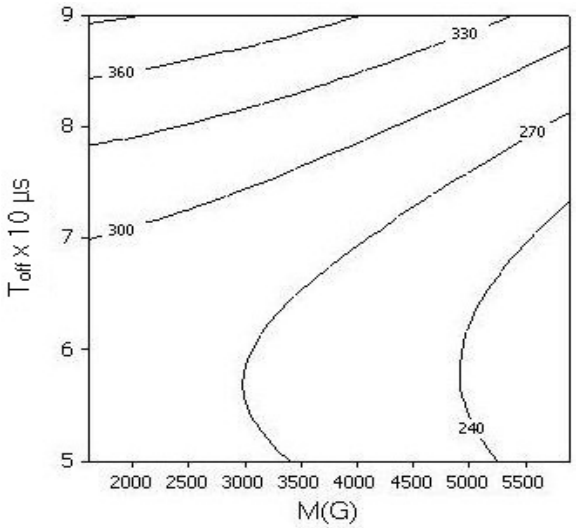

(c) low hold values

Figure 4.8: Response Plots of MRR vs T_{off}, M

The interaction effect of Pulse-off time and Magnetic intensity on MRR, with hold values at low setting, is shown in Figure 4.8c. Highest MRR values(≥360-390mg/min) are seen at T_{off} values above 85μs and magnetic intensity levels below 3500G.

The above results show that high MRR levels are obtained when T_n and I are at high hold values (T_n=90μs, I=23.44A) and M≥4000G, T_{off}≤50μs.

Figure 4.9 shows the interaction effect of current (I) and magnetic field intensity(M) on MRR.

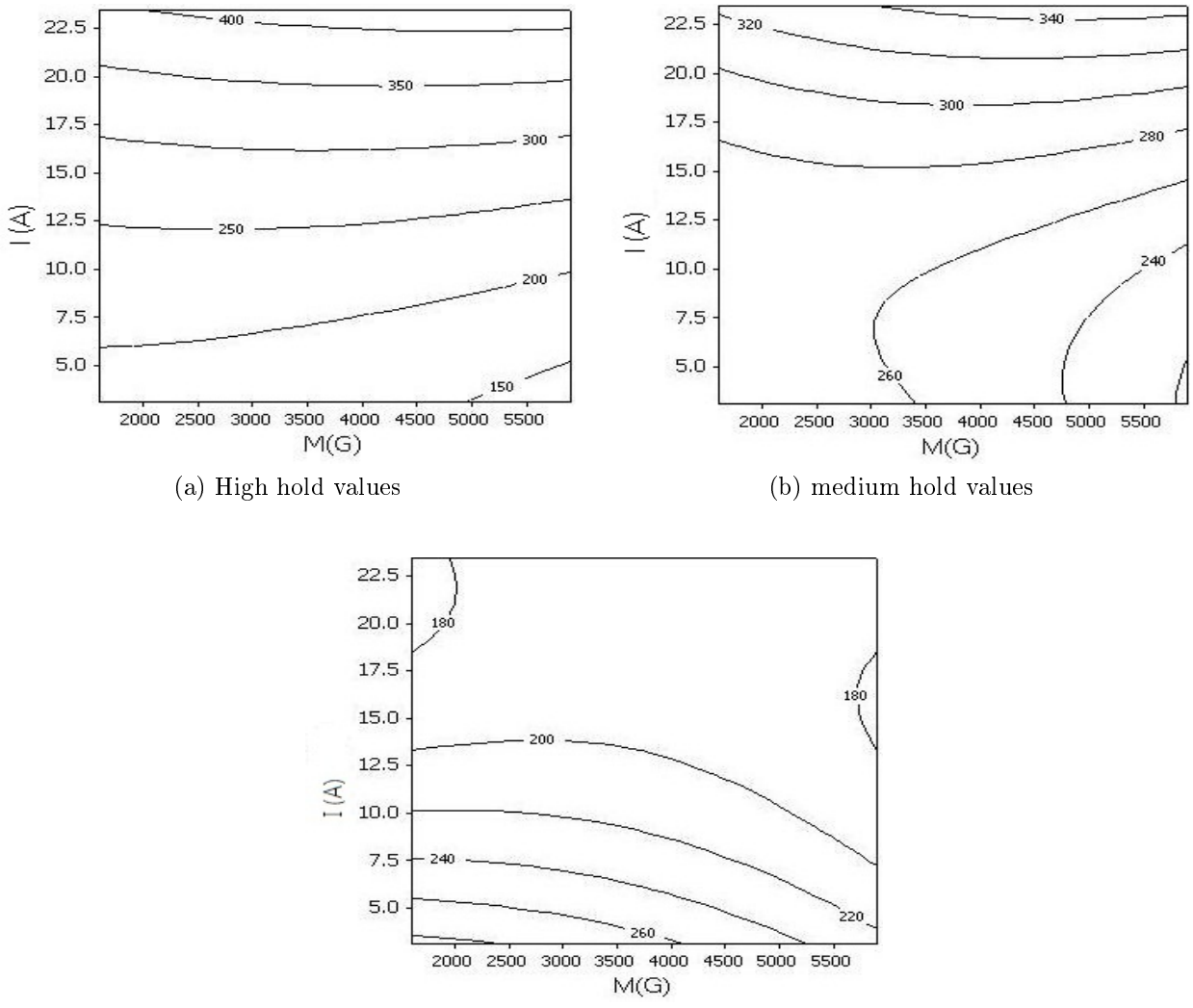

(a) High hold values

(b) medium hold values

(c) low hold values

Figure 4.9: Response Plot of MRR vs I, M

High MRR levels($\geq$400mg/min) are observed at maximum current (22.5A) and maximum magnetic intensity($\geq$5000G). At medium hold values, high MRR ($\geq$340 mg/min) are observed at maximum current(22.5A) and magnetic intensity $\geq$3000G. At low hold values high MRR($\geq$260 mg/min) is observed at low current($\leq$5A) and low magnetic intensity($\leq$3500G). The results show that high material removal rates are obtained when T_n and T_{off} are at high hold values (T_n=90μs,T_{off}=90μs) and M$\geq$2500G, I$\geq$22.5A.

Figure 4.10 shows the interaction effect of Pulse-on time (T_n) and Pulse-off time (T_{off}) on MRR. The highest MRR value ($\geq$400mg/min)is observed when the pulse-on time is at its higher setting ($\geq$90 μs) and pulse-off time is either at high levels ($\geq$ 80μs) or at its low levels($\leq$60μs). With medium hold levels, the maximum MRR values ($\geq$325mg/min) are observed when T_n is between 60 μs and 85 μs and Tf is at high levels ($\geq$ 85μs). At low hold values, Figure 4.10c, the maximum MRR values($\geq$350mg/min) are observed when the pulse-on time is at its low settings($\leq$70 μs) and pulse-off time at high levels($\geq$80μs).

High material removal rates are attained when current and magnetic intensity are at maximum values i.e. I=23.44A and M=5903(G) and T_n ($\geq$90 μs) and pulse-off time is either at high levels ($\geq$ 80μs) or at its low levels ($\leq$60μs).

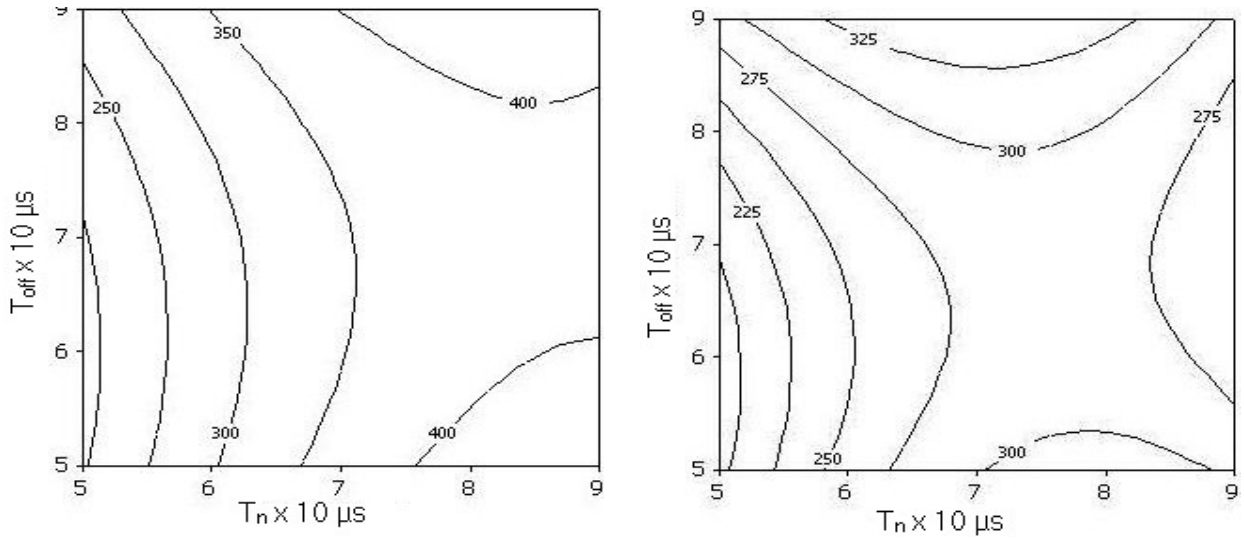

(a) High hold values

(b) medium hold values

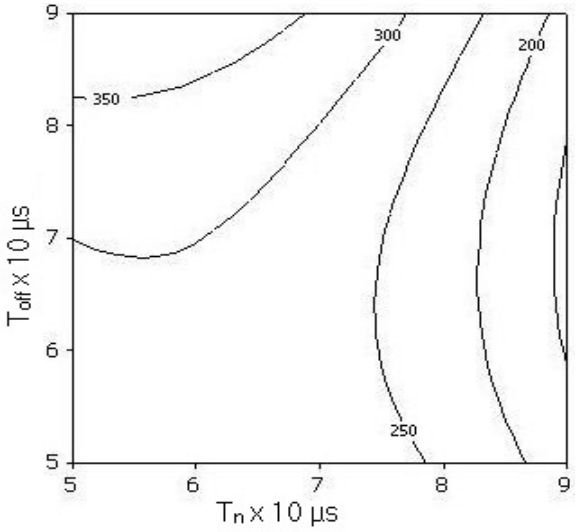

(c) low hold values

Figure 4.10: Response Plot of MRR vs T_n, T_{off}

Figure 4.11 shows the interaction effect of Pulse-on time(T_n) and current(I) on MRR at the three hold values. At high hold settings high material removal rates ($\geq$400mg/min) are observed at high pulse-on time levels($\geq$70 μs) and current values of above 22.5A. At medium hold levels,the maximum MRR values($\geq$350mg/min) are observed at high pulse-on

time levels($\geq$75 μs) and current values of above 22.5A. Figure 4.11c shows the interaction

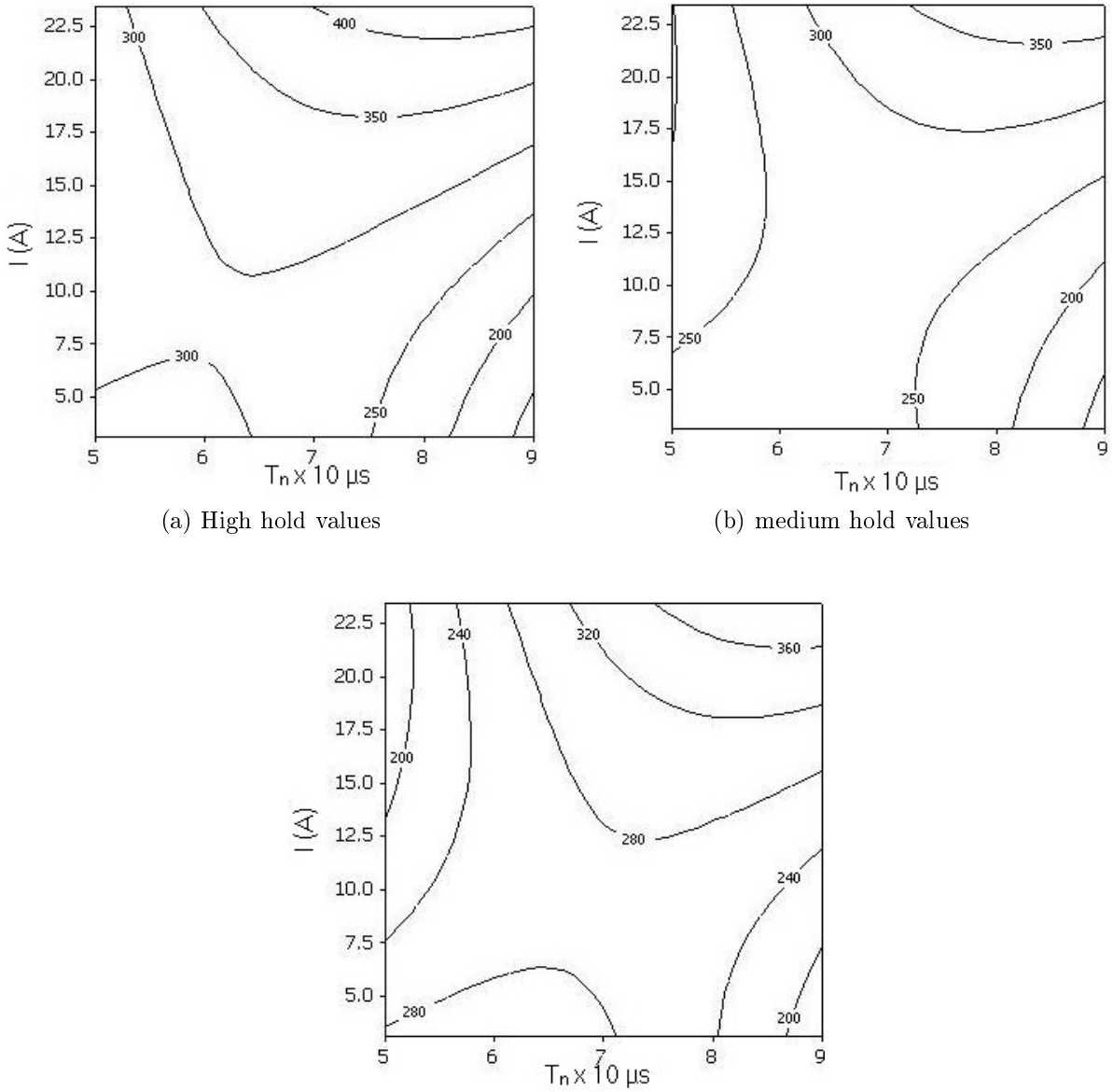

(a) High hold values

(b) medium hold values

(c) low hold values

Figure 4.11: Response Plot of MRR vs Tn, I

effect of Pulse-on time(T_n) and current(I) on MRR at low hold values. High material removal rates ($\geq$360mg/min) are observed at high pulse-on time levels($\geq$75 μs) and current values of above 21A.

In this case, the best (highest) values of MRR are attained when the pulse-off time and magnetic intensity are set on their highest values and pulse-on time is maintained at values($\geq$70 μs) and current values of above 22.5A.

The interaction effect of Pulse-off time(T_{off}) and current(I) on MRR is shown in Figure 4.12.

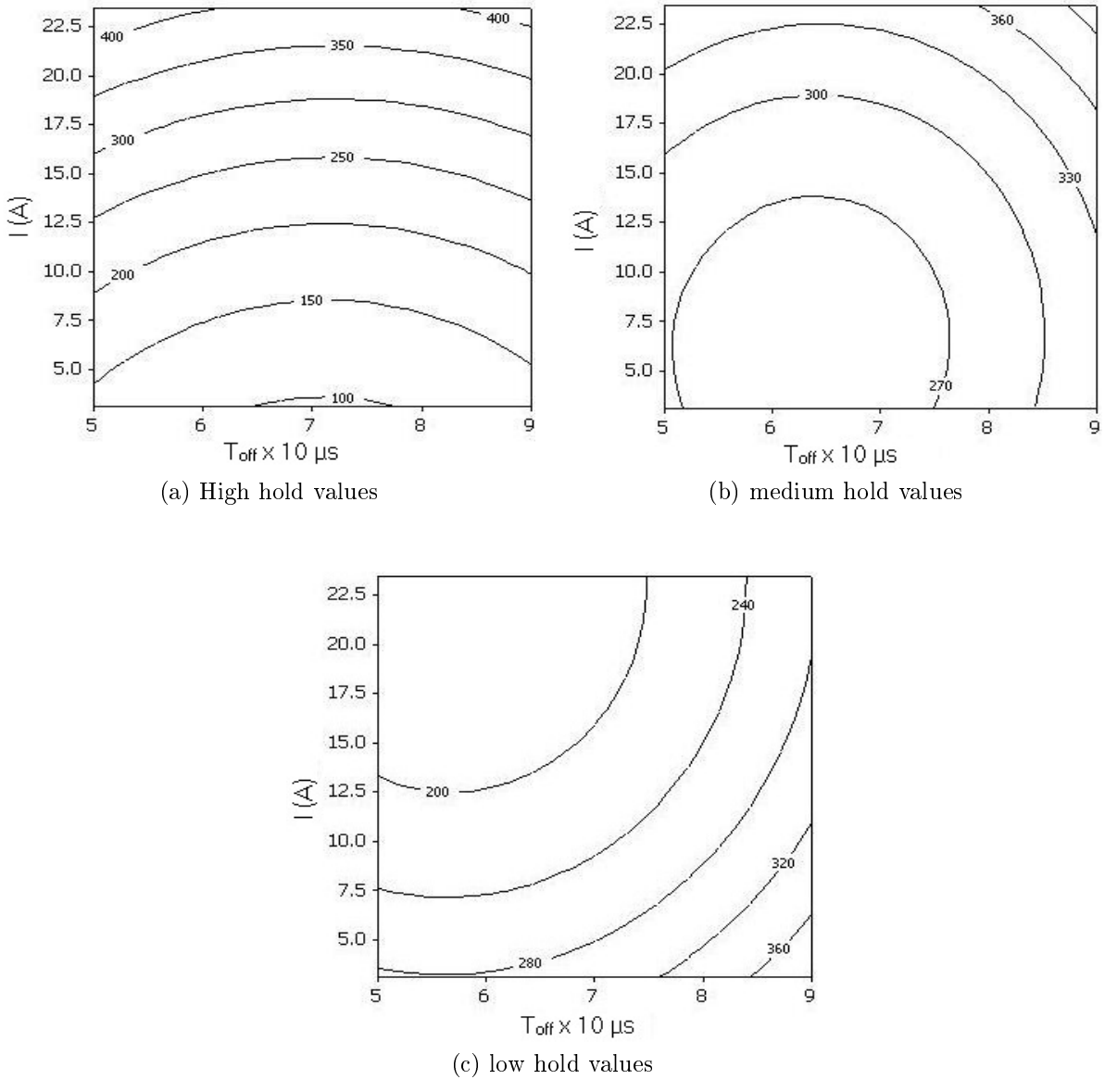

(a) High hold values

(b) medium hold values

(c) low hold values

Figure 4.12: Response Plot of MRR vs T_{off}, I

High material removal rates ($\geq$400mg/min) are observed at current levels $\geq$21.0A and at either

low T_{off} ($\leq$60 μs) or high T_{off} ($\geq$85μs). At medium hold values, the high MRR values i.e. above 360mg/min are observed at current levels above 20.0 A and at high pulse-off time ($\geq$80 μs). At low hold values, Figure 4.12c, the maximum MRR values($\geq$320mg/min) are observed at current levels below 7.5 A and at high T_{off}($\geq$80 μs).

The maximum MRR values in this case are attained when T_n and M are set at their maximum values i.e. 90μs and 5903G respectively. On the other hand the current should be set at levels $\geq$21.0A and low T_{off} ($\leq$60 μs).

The optimum results for the various cases above indicate that in overall, to obtain high material removal rates, one is required to set the magnetic intensity, pulse-on time and current on their maximum values and retain pulse-off time at its lowest value.

This Conclusion is further affirmed using a response optimizer algorithm implemented using the statistical software. Figure 4.13 shows the results obtained by setting a target value of 300 mg/min and a lower value of 200mg/min for the optimization.

Minitab employs a reduced gradient algorithm with multiple starting points that maximizes the composite desirability to determine the numerical optimal solution (optimal input variable settings). The results show that a maximum material removal rate of 436.8626mg/min, is attainable if the magnetic intensity, pulse-on time and current are set at their maximum values i.e. 5903G, 90μs and 23.4375A respectively (indicated in red). The pulse-off time should be set at its lowest value i.e. 50μs.

Individual desirability (d) evaluates how the settings optimize a single response; composite desirability (D) evaluates how the settings optimize a set of responses overall. Desirability has a range of zero to one. One represents the ideal case; zero indicates that one or more responses

are outside their acceptable limits.

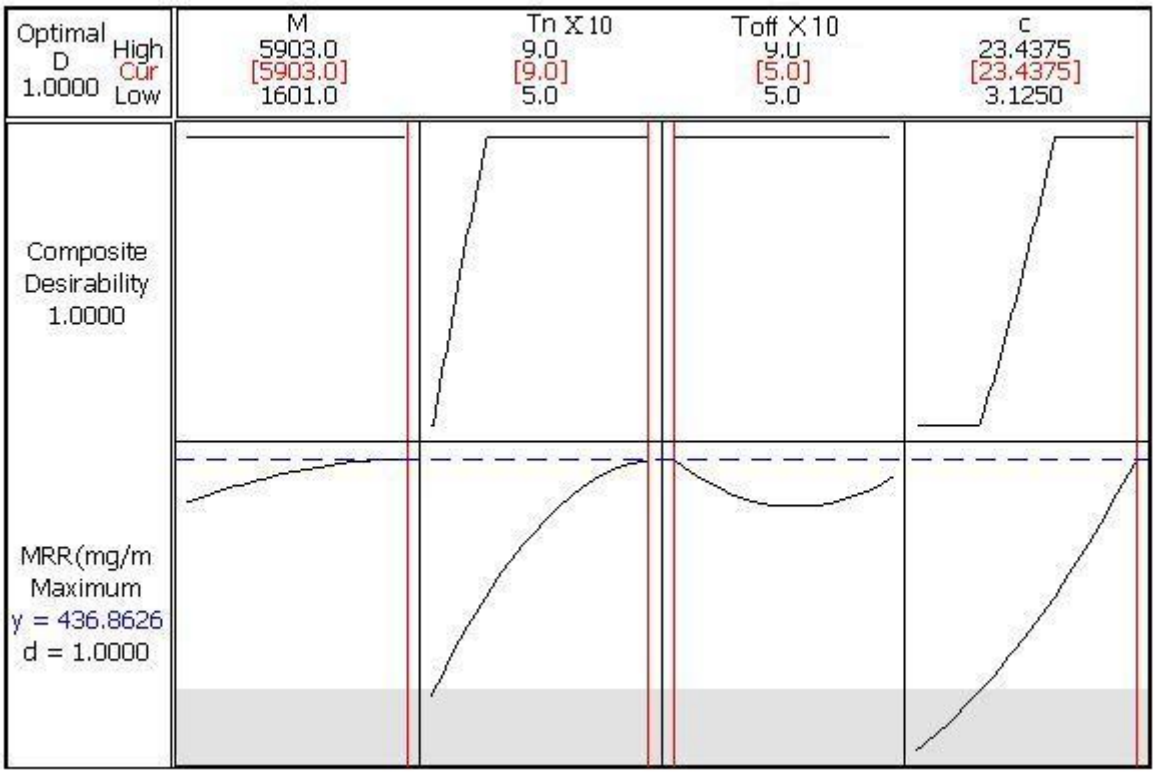

Figure 4.13: Statistical response optimization of MRR

4.2.2 Ra response analysis

Table 4.10 shows the factors interactions considered for Ra and their confidence levels. The significance level of the interaction between current and pulse-on time is high(90.7%). This shows a high dependence level between the two.

Table 4.10: Interactions and confidencle levels

Interaction	Confidence level
T_n - M	66.5
T_{off} - M	35.9
I - M	32
T_{off} - T_n	12.5
I - T_n	90.7
I - T_{off}	88.3

Figure 4.14 shows the response surface for Ra in relation to magnetic intensity (M) and pulse-on time(T_n). It can be seen that the Ra is more affected by the pulse-on time as opposed to magnetic intensity. However at high magnetic intensity and pulse-on time, the surface roughness is noted to be at its highest level. Low Ra values($\leq$5 μm) are attained at low T_n($\leq$55μs)and high magnetic intensities($\geq$4600G). At medium hold values, low Ra ($\leq$9μm)are observed at low T_n($\leq$5.5A)and high M values($\geq$3600G). Figure 4.14c shows the response surface for Ra in relation to the design parameters of magnetic intensity and pulse-on time at low hold values. Low Ra is observed at high T_n ($\geq$80μs) and low M values($\leq$3000G)

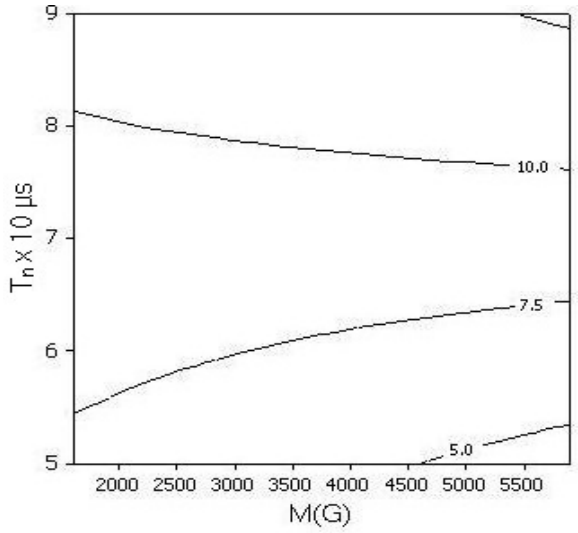

(a) High hold values

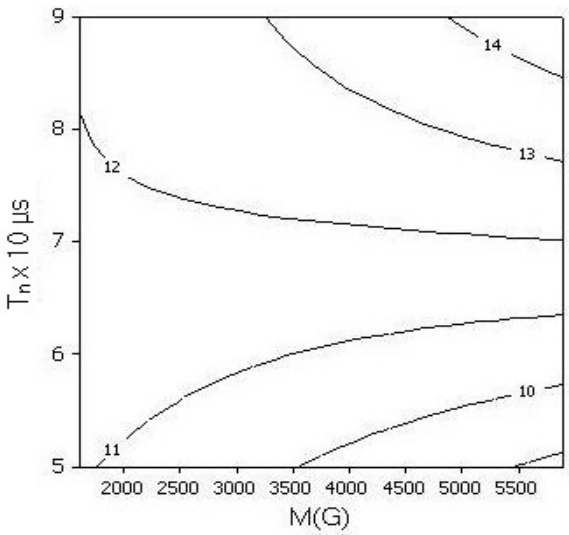

(b) medium hold values

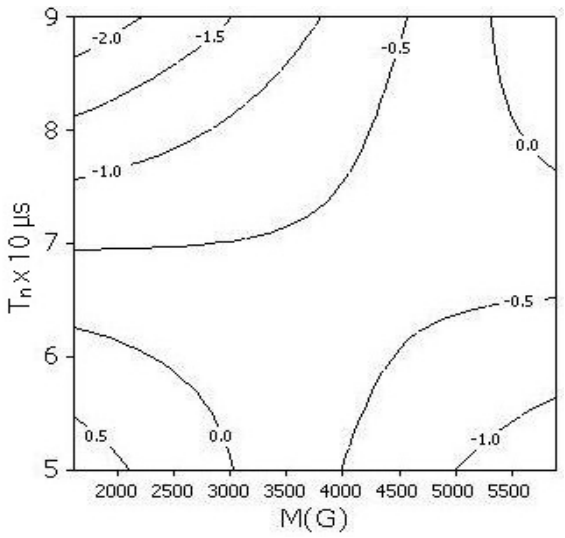

(c) low hold values

Figure 4.14: Response Plot of Ra vs T_n, M

The lowest (optimum) Ra values, are obtained at low $T_n(\leq 55\mu s)$and high magnetic intensities($\geq$4600G) with T_{off} and current set at their maximum values.

The interaction effect of Pulse-off time (T_{off}) and Magnetic intensity (M) on Ra , is shown in Figure 4.15. It is observed that the value of Ra increases with increase in magnetic intensity.

Minimum Ra values (10-11μm) is seen at low T_{off} values($\leq$60μs) and at low magnetic intensities ($\leq$2800G). At medium hold values, minimum roughness(9 to 9.5μs) values are attained at low Tf ($\leq$60μs) and low magnetic intensity ($\leq$3500G).

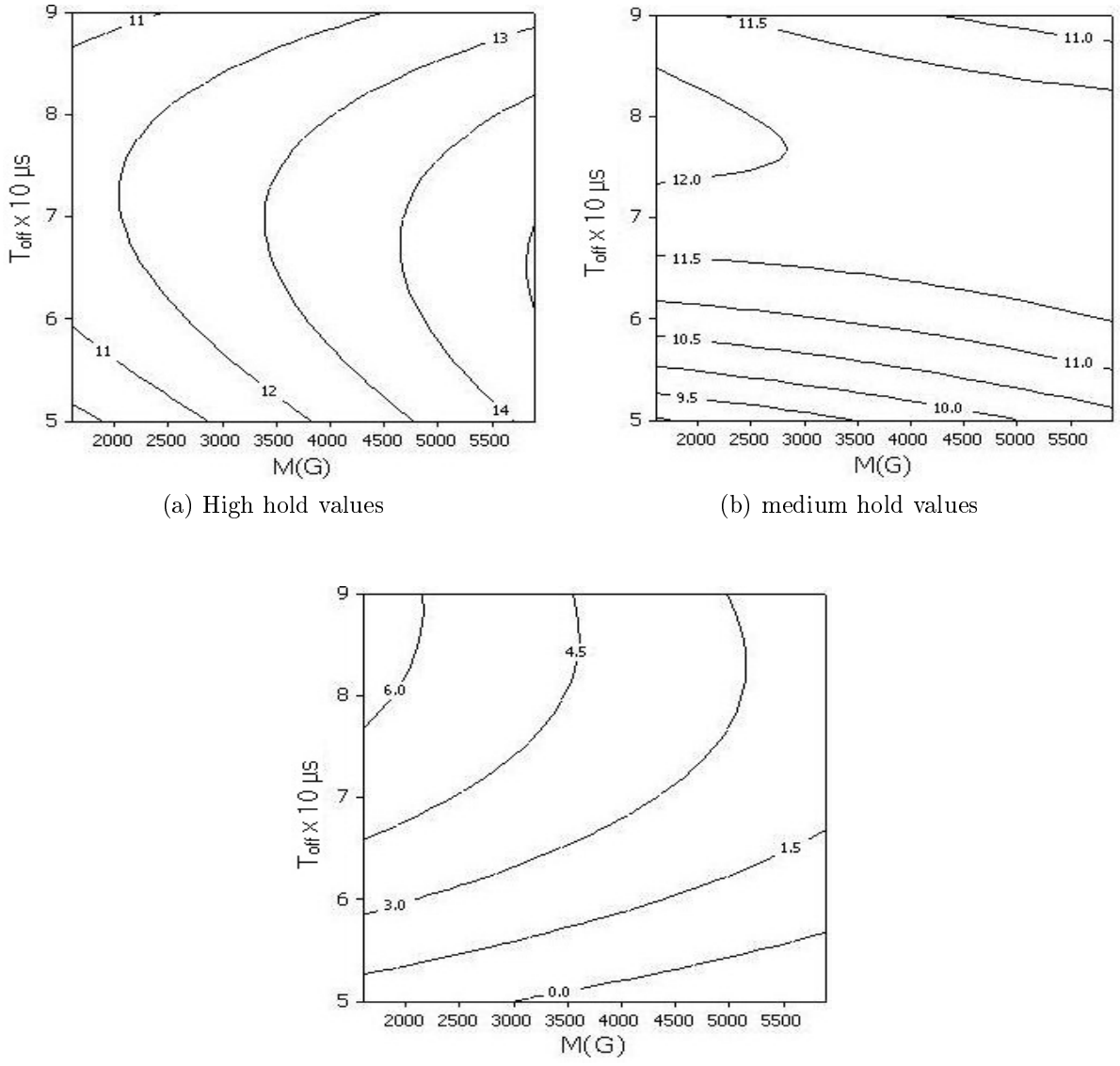

(a) High hold values

(b) medium hold values

(c) low hold values

Figure 4.15: Response Plots of Ra vs T_{off}, M

At low hold values, Figure 4.15c, minimum roughness values($\leq$1.5μm) are attained at low T_{off}($\leq$5.5μs) and high magnetic intensity($\geq$3500G).

The optimum values for the parameter Ra are obtained at low T_{off} ($\leq$5.5μs) and high magnetic intensity ($\geq$3500G) with current and pulse-on time set at minimum i.e. 3.125A and 50 μs respectively.

The interaction effect of current (I) and magnetic field intensity(M) on Ra is shown in Figure 4.16.

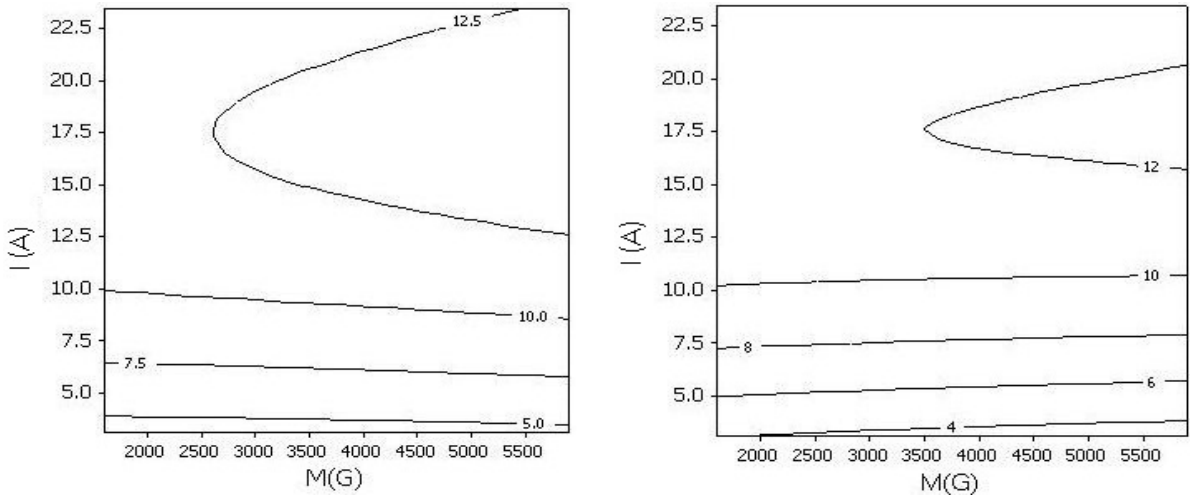

(a) High hold values

(b) medium hold values

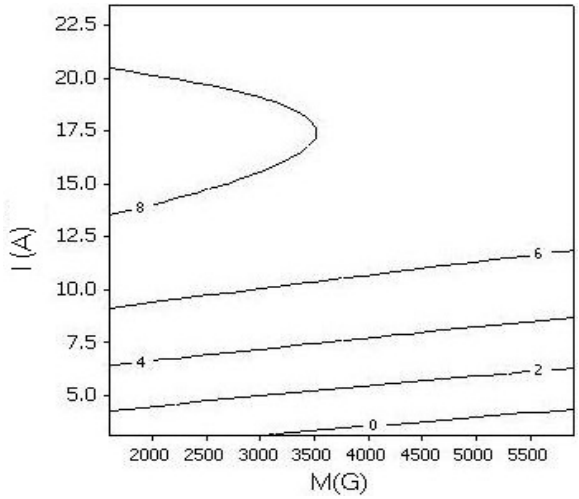

(c) low hold values

Figure 4.16: Response Plots of Ra vs I, M

Low Ra values($\leq$5.0μm) are observed when the current is set below 5A. High magnetic intensities at high currents are seen to produce rougher surfaces. At medium hold values, Ra is seen to be more dependent on current and the minimum roughness values ($\leq$4μm) are observed at C$\leq$5.0A.

Figure 4.16c shows the interaction effect of current (I) and magnetic field intensity (M) on Ra at low hold values. The minimum roughness($\leq$2μm) are observed at C$\leq$5.5A. Current values lesser than 5A are seen to produce minimum roughness on workpieces and in this case the magnetic intensity does not influence heavily on Ra.

The interaction effect of Pulse-on time(T_n) and Pulse-off time(T_{off}) on Ra is shown in Figure 4.17. It is observed that Ra is highly influenced by pulse-on time and it increases as T_n rises. Minimum Ra values($\leq$75μm) are attained at low T_n($\leq$55μs). At medium hold values, low roughness values($\leq$80μm) are observed at low T_n and T_{off} values.

Figure 4.17c shows the interaction effect of Pulse-on time(T_n) and Pulse-off time(T_{off}) on Ra at low hold values. Low roughness values($\leq$2μm) are observed at low Tf($\leq$60μs).

These results show that the optimum values of surface roughness are observed at low Pulse-on time ($\leq$60μs)

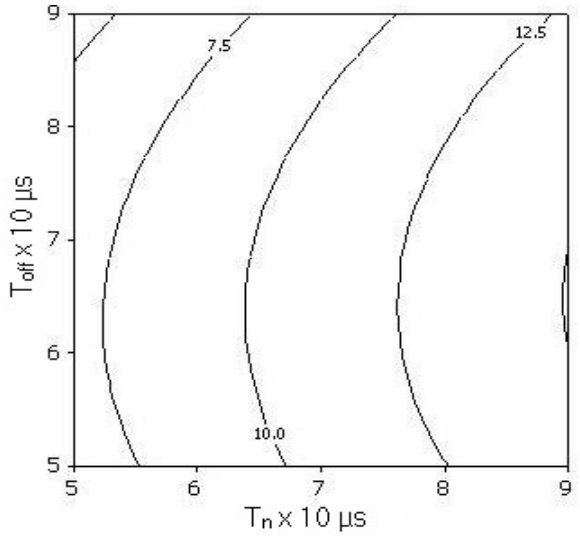

(a) High hold values

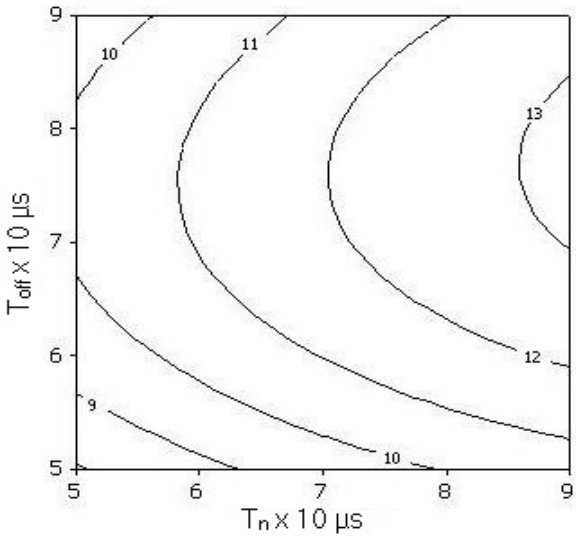

(b) medium hold values

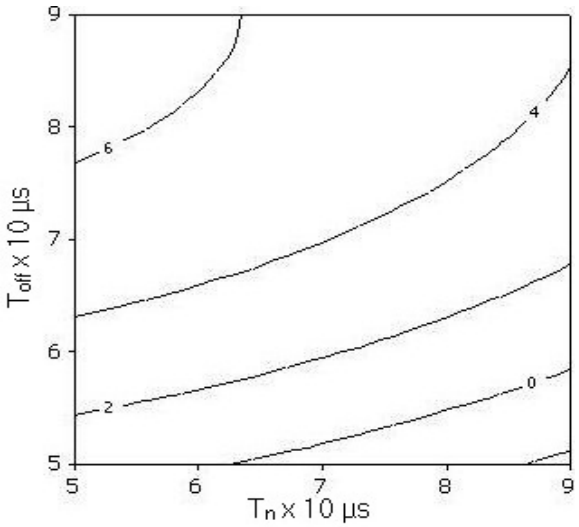

(c) low hold values

Figure 4.17: Response Plots of Ra vs T_n, T_{off}

Figure 4.18 shows the interaction effect of Pulse-on time(T_n) and current (I) on Ra. The minimum Ra values($\leq 4\mu$m) are observed when Tn values are below 70μs and the current is below 5.0A. At medium levels, minimum Ra values($\leq 6\mu$m) are observed when the current remains below 5.0A. At low hold levels, Figure 4.18c, minimum Ra values($\leq 2.5\mu$m) are observed when the current remains below 5.0A.

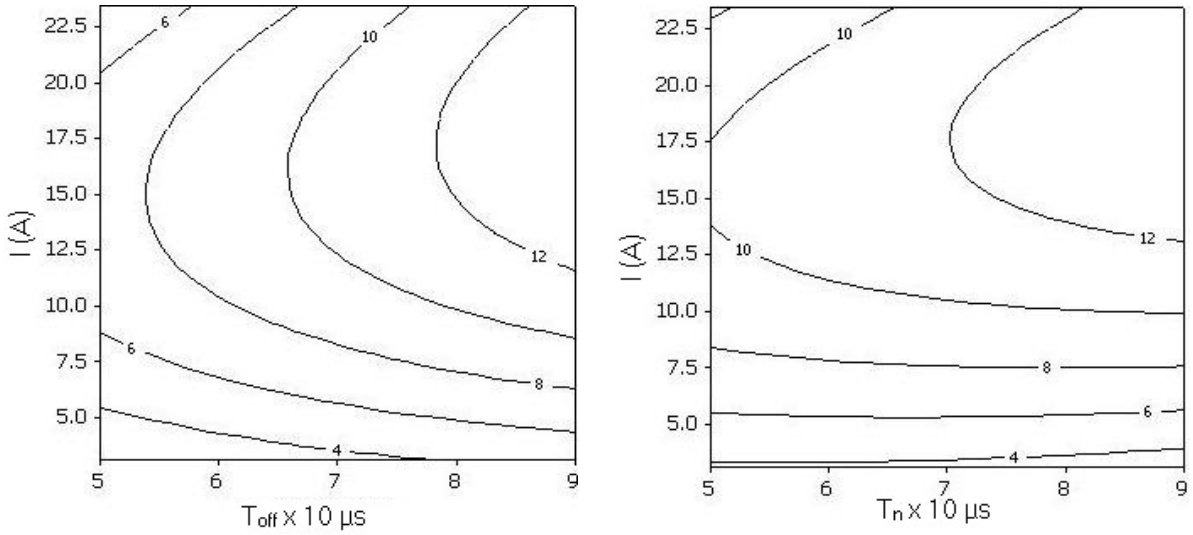

(a) High hold values

(b) medium hold values

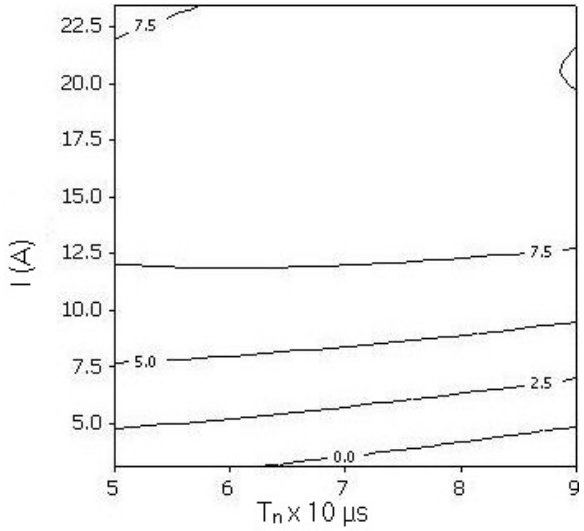

(c) low hold values

Figure 4.18: Response Plots of Ra vs T_n, I

For minimum roughness, the current should be maintained below 5A, with magnetic intensity and pulse-off time maintained at minimum values i.e. 1601G and 50μs respectively.

Figure 4.19 shows the interaction effect of Pulse-off time(T_{off}) and current(I) on Ra. High roughness values($\geq$14μm) are observed when current values exceed 15A and the pulse-off time remains below 9 μs. At medium hold values, low roughness values ($\leq$2μm) are observed when current values are below 5.0A and the pulse-off time remains below 6 μs. At low hold values, Figure 4.19c, low roughness values ($\leq$4μm) are observed when current values are below 5.5A and the pulse-off time remains below 6 μs.

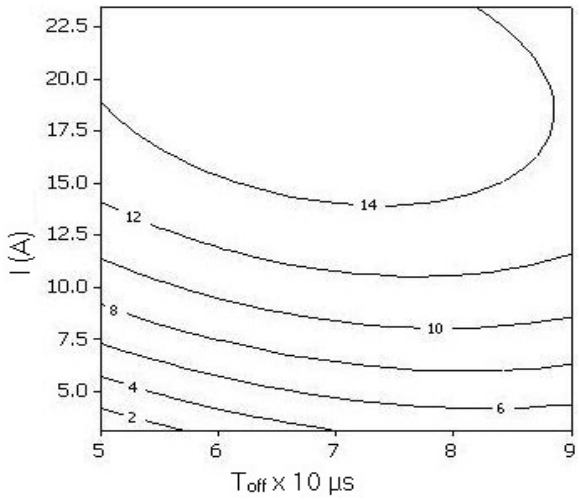

(a) High hold values

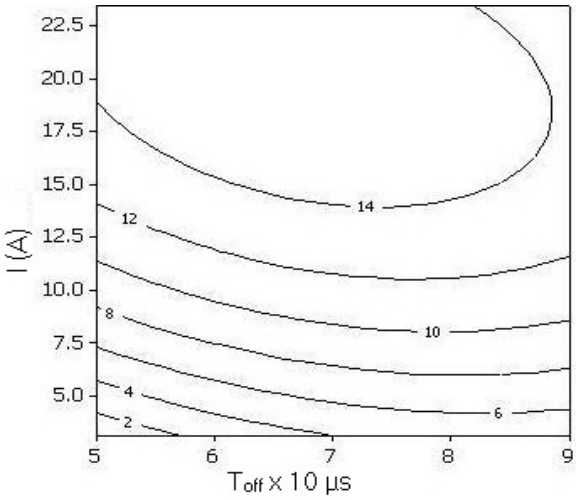

(b) medium hold values

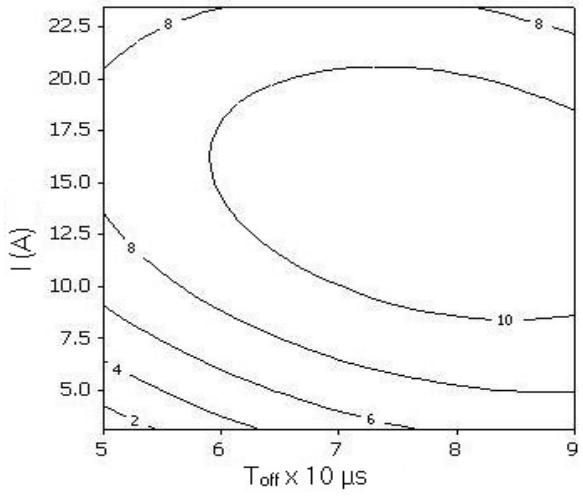

(c) low hold values

Figure 4.19: Response Plots of Ra vs T_{off}, I

It is observed again that low roughness values are attained when the current remains below 5 A, magnetic intensity is at 3309G and pulse-on time is at 50μs. Pulse-off time does not influence this parameter considerably.

From the results for the individual cases above, it is clear that current levels must be low ($\leq$6A) for low roughness on work pieces. The other settings are seen to vary for the different cases. Statistical optimization confirms the assertion that current should be low for smoother surfaces. Figure 4.20 shows that an optimum level of 4μm can be reached by setting the magnetic intensity level and pulse-on time at their maximum values(i.e. 5903G and 90μs). The pulse-off time should be set at 58.826μs and the current at 4.3243A.

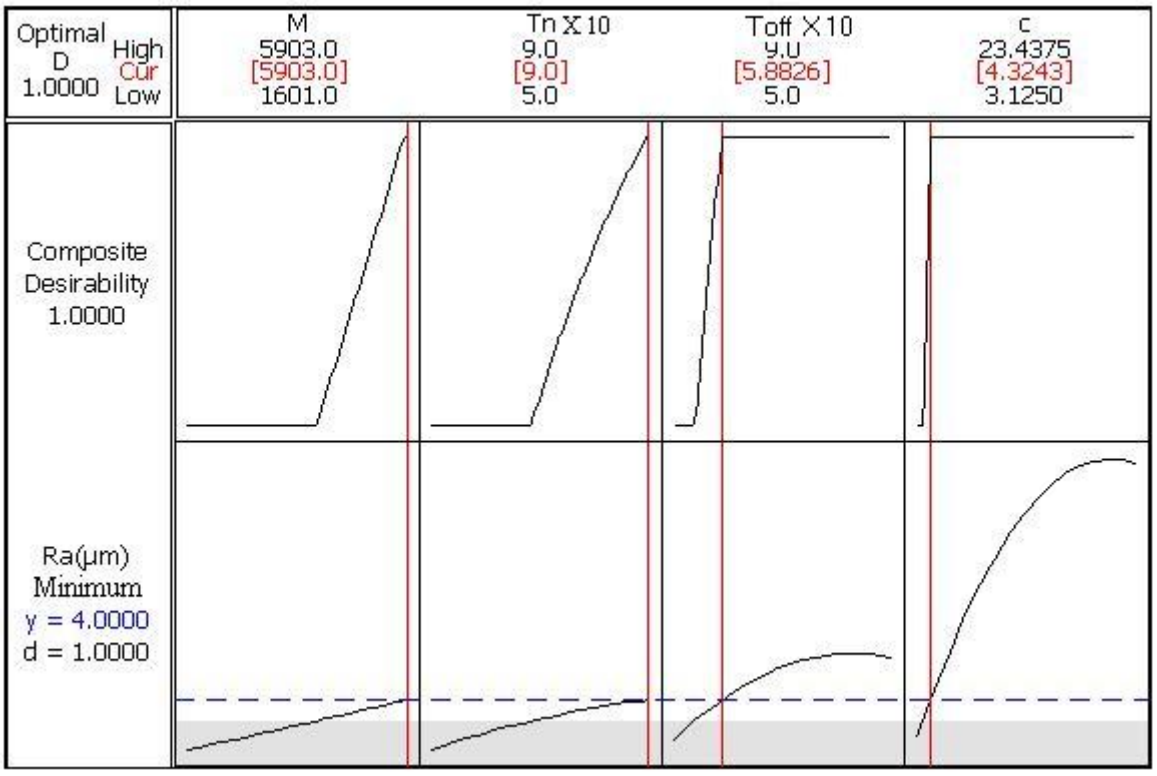

Figure 4.20: Statistical response optimization of Ra

4.2.3 TWR response analysis

Table 4.11 shows the factors interactions considered for Ra and their confidence levels. Once

Table 4.11: Interactions and confidencle levels

Interaction	Confidence level
T_n - M	6.3
T_{off} - M	2.1
I - M	44
T_{off} - T_n	57.9
I - T_n	99.3
I - T_{off}	24.3

again it is observed that the dependence level between current and pulse-on time is very high at a significance level of almost 100%.

Figure 4.21 shows the response surface for TWR in relation to the design parameters of magnetic intensity (M) and pulse-on time (T_n). The TWR is more dependent on Tn as opposed to the magnetic influence at the maximum hold values. Low tool wear rates ($\leq$12mg/min) are observed at pulse-on time settings of between 75μs and 80μs and at magnetic intensity levels of above 5000G. At medium hold values, the TWR is again observed to be more dependent on Tn as opposed to the magnetic influence. Low wear rates ($\leq$15.5 mg/min) are experienced at pulse-on time settings of between 65μs and 85μs. Figure 4.21c shows the response surface at low hold values. Low tool wear rates ($\leq$15mg/min) are observed at $T_n \leq$ 8.0μs and M$\leq$4700G.

For this case, the lowest tool wear rate is attained at pulse-on time settings of between 75μs and 80μs and at magnetic intensity levels of above 5000G with current set at maximum(23.437A) and pulse-off time at medium settings(50μs).

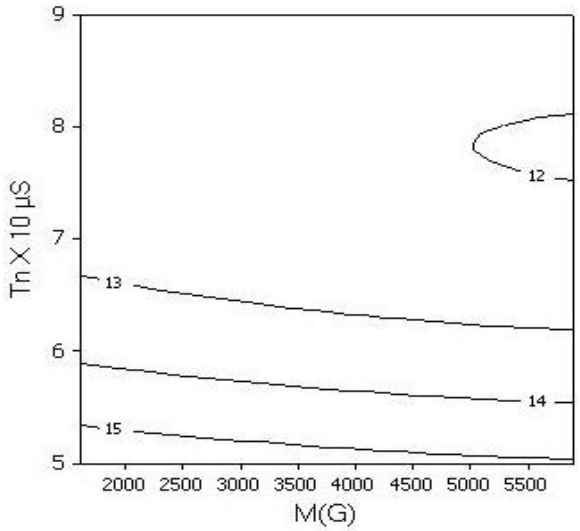

(a) High hold values

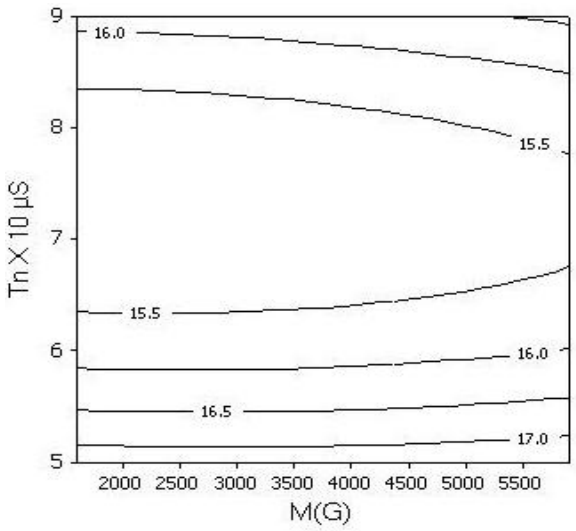

(b) medium hold values

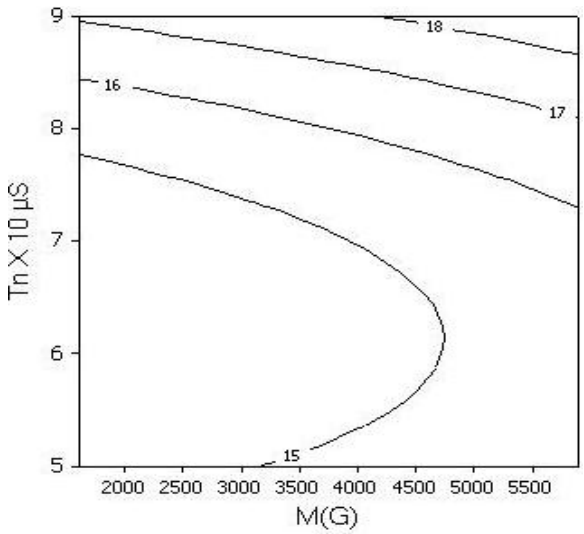

(c) low hold values

Figure 4.21: Response Plots of TWR vs Tn, M

The interaction effect of Pulse-off time(T_{off}) and Magnetic intensity (M) on TWR is shown in Figure 4.22. Minimum tool wear rates($\leq$12.50mg/min) are experienced when the magnetic intensity is set above 5000G and the pulse-off time is either at above 85μs or below 55μs. At medium hold values, minimum tool wear rates($\leq$14.75mg/min) are experienced when the pulse-off time is below 55μs.

At low hold values, Figure 4.22c, minimum tool wear rates($\leq$15mg/min) are experienced when

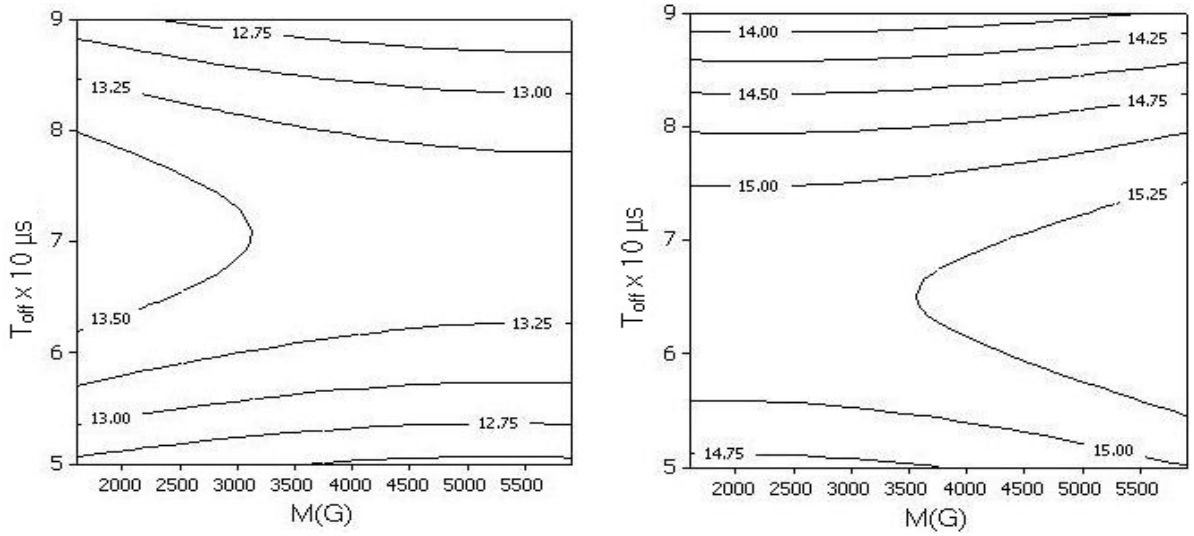

(a) High hold values

(b) medium hold values

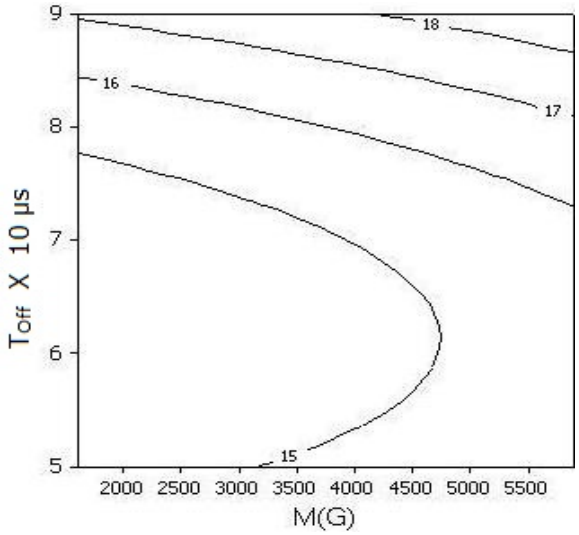

(c) low hold values

Figure 4.22: Response Plots of TWR vs T_{off}, M

the pulse-off time is $\leq$80μs and magnetic intensity is below 4500G.

The best configuration for attaining low TWR entails setting the magnetic intensity above 5000G and the pulse-off time is either at above 85μs or below 55μs. Also, the current and

pulse-on time should be set at their maximum values i.e. 23.437A and 90 μs.

Figure 4.23 shows the interaction effect of current (I) and magnetic field intensity(M) on TWR.

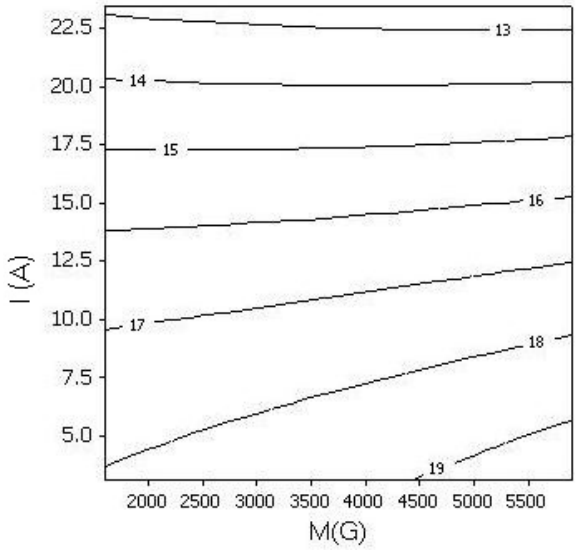

(a) High hold values

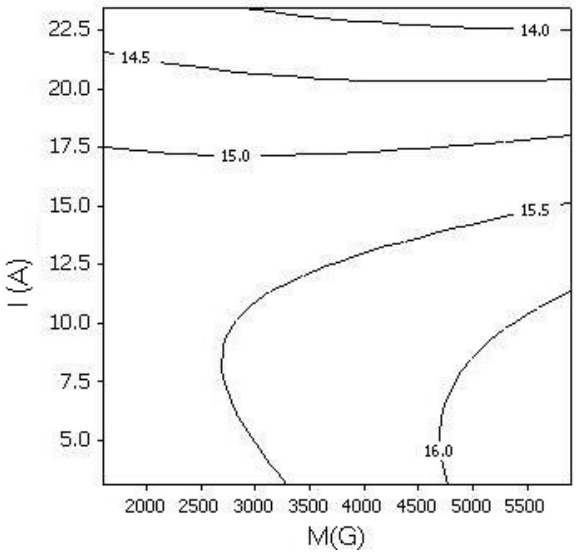

(b) medium hold values

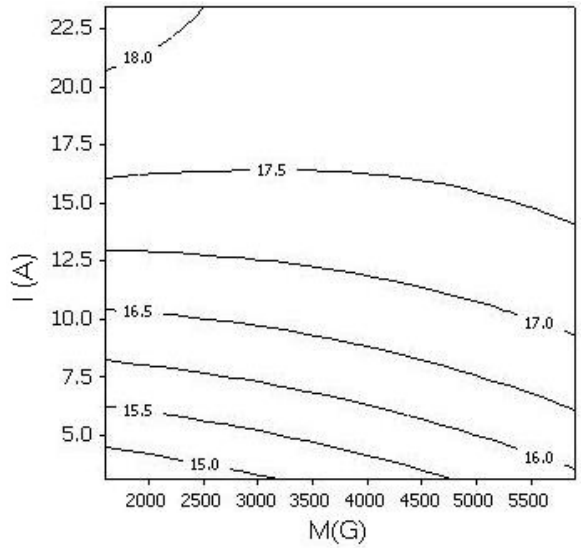

(c) low hold values

Figure 4.23: Response Plots of TWR vs I, M

Settings of magnetic intensity that supersede 4500G at current levels below 5A, result in high TWR($\geq$19mg/min). At medium hold values, for minimum TWR($\leq$14.5mg/min), the current should be set above 21.0A and magnetic intensity above 4000 Figure 4.23c shows the interaction effect of current and magnetic field intensity on Ra at low hold values. For minimum TWR($\leq$15.5mg/min), the current should be set below 5.5A and magnetic intensity below 4500G.

Current levels above 22.5A, result in the lowest tool wear rate with the pulse-on time and pulse-off time set at their maximum values(90μs). Magnetic intensity does not influence the TWR in this case.

The interaction effect of Pulse-on time(T_n) and Pulse-off time(T_{off}) on TWR is shown in Figure 4.24. For minimum tool wear rate($\leq$12 mg/min),the pulse-on time should be set to levels above 70μs and pulse-off time maintained at either $\geq$80μs or $\leq$60μs. At medium hold values, for minimum tool wear rate($\leq$15mg/min),the pulse-on time should be set to levels between 65μs and 87μs and pulse-off time maintained at either $\geq$75μs or $\leq$55μs.

At low hold values, Figure 4.24, for minimum tool wear rate($\leq$14mg/min), the pulse-on time should be set to levels below 70μs and pulse-off time above 80 μs.

For optimum TWR, the pulse-on time should be set to levels above 70μs and pulse-off time maintained at either $\geq$80μs or $\leq$60μs. The current and magnetic intensity should be set at their maximum values.

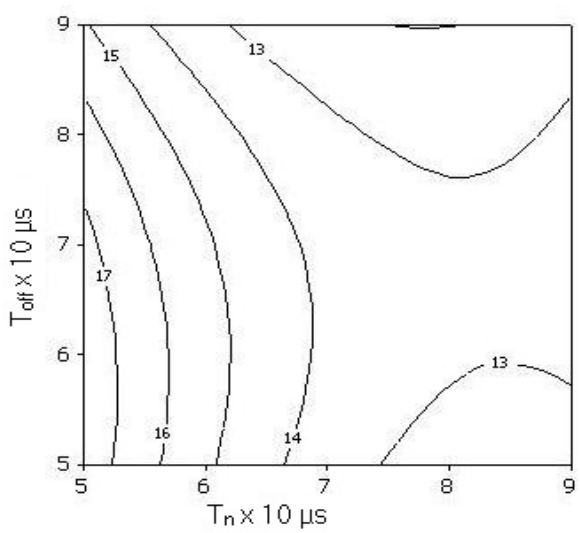

(a) High hold values

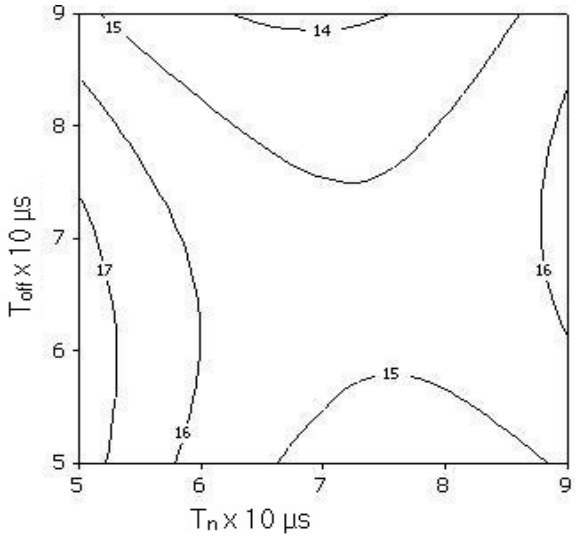

(b) medium hold values

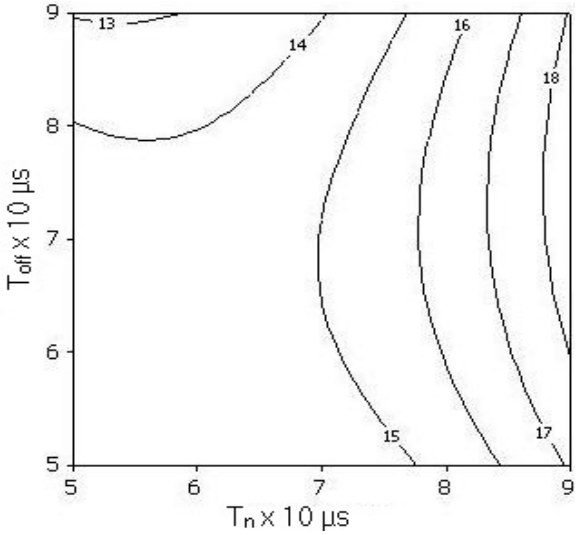

(c) low hold values

Figure 4.24: Response Plots of TWR vs Tn, T_{off}

Figure 4.25 shows the interaction effect of Pulse-on time(T_n) and current(I) on TWR. For minimum tool wear rate($\leq$12mg/min), the pulse-on time should be greater than 60μs with the current being set at levels above 18A. At medium hold values, for minimum tool wear rate($\leq$14 mg/min), the pulse-on time should be greater than 70μs with the current being set

at levels above 21A.Figure 4.25c shows the interaction effect of Pulse-on time and current on TWR at low hold values. For minimum tool wear rate($\leq$13 mg/min), the pulse-on time should be greater than 80μs with the current being set at levels above 22.5A.

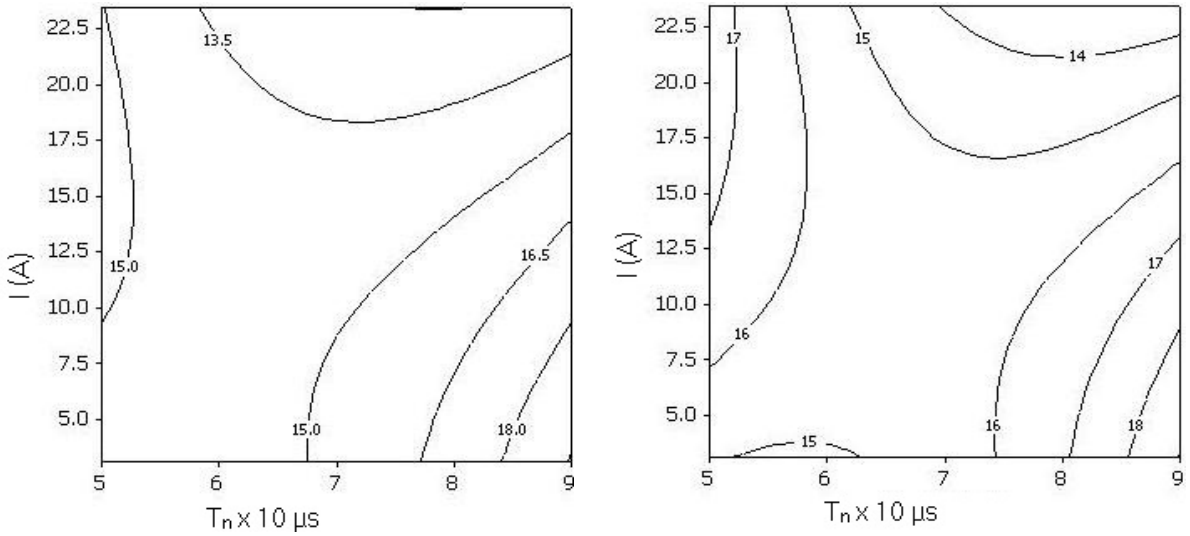

(a) High hold values

(b) medium hold values

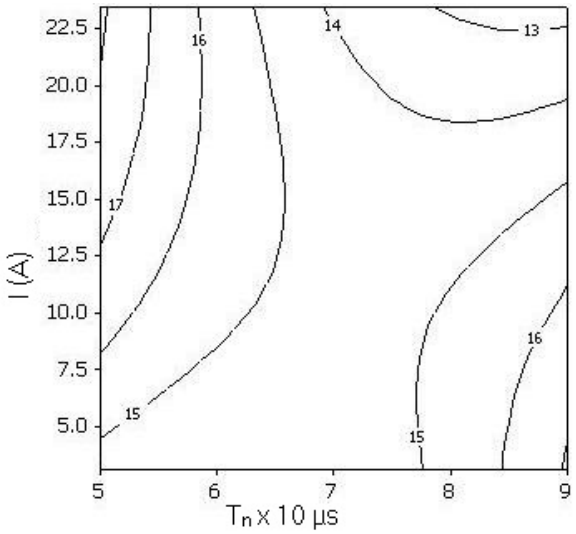

(c) low hold values

Figure 4.25: Response Plots of TWR vs Tn, I

From the above results it can be seen that the minimum TWR is obtained when the pulse-on time is greater than 60μs with the current being set at levels above 18A and magnetic intensity and pulse-off time at their maximum values.

The interaction effect of Pulse-off time(T_{off}) and current(I) on TWR is shown in Figure 4.26.

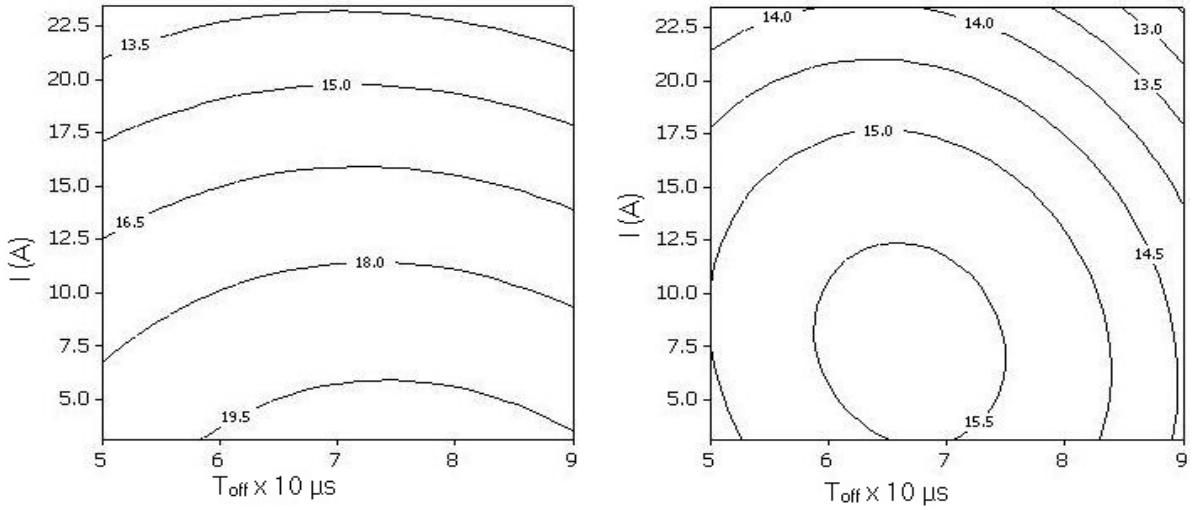

(a) High hold values

(b) medium hold values

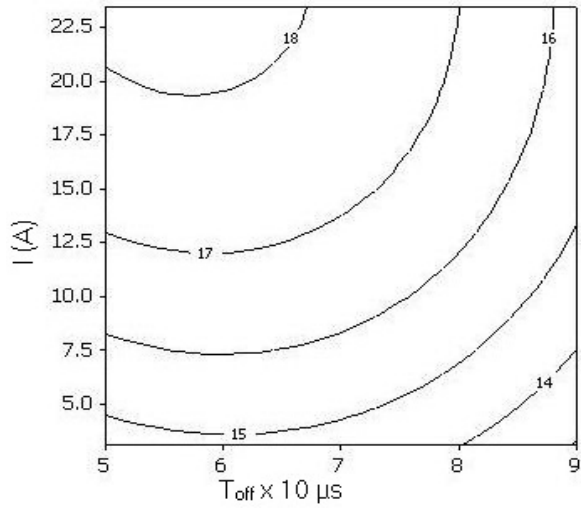

(c) low hold values

Figure 4.26: Contour Plot of TWR vs T_{off},I

Low TWR is observed when the current levels are above 20.5 and the pulse-off time is set at either $\leq 60\mu$s or $\geq 80\mu$s. At medium hold values, the minimum TWR ($\leq$13mg/min)is observed when the current levels are above 20.5 and the pulse-off time is $\geq 80\mu$s.

At low hold values, Figure 4.26c, the minimum TWR (13-14mg/min)is observed when the current levels are below 75 and the pulse-off time is $\geq 80\mu$s.

For this case, the optimum TWR values are obtained when the current levels are above 20.5 and the pulse-off time is $\geq 80\mu$s. The magnetic intensity and pulse-off time are set to their medium hold value.

It can be concluded from the results for the individual cases above that in order to obtain the minimum tool wear rates the current has to be above 22A, the pulse-on time should be at an average of 75μs, the pulse-off time should be high and the magnetic intensity at the maximum setting i.e. 5500G.

This Conclusion was backed-up with the results obtained after running the statistical optimization.Figure 4.27 shows the results obtained by setting a target value of 13 mg/min and an upper value of 15 mg/min for the optimization.

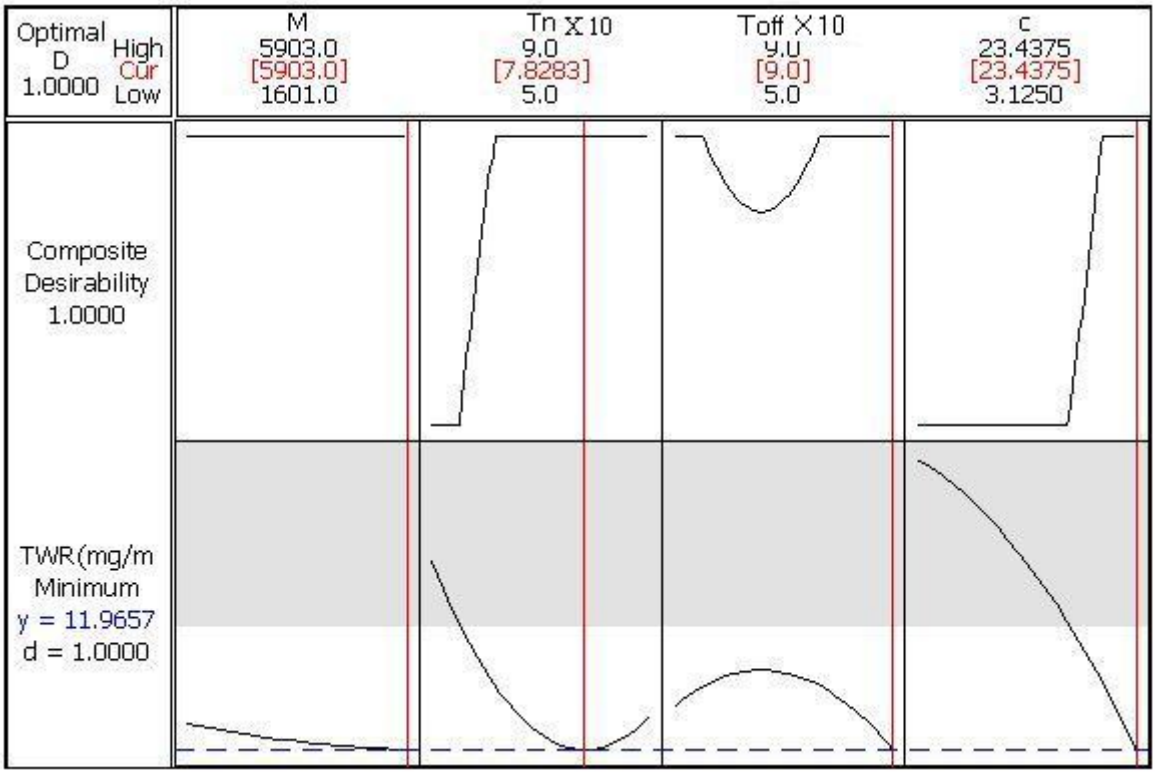

Figure 4.27: Statistical response optimization of TWR

The best value attaintable for tool wear rate is 11.9657 mg/min. This is after setting the magnetic intensity 5903G, the pulse-on time at 7.823μs, pulse-off time at 5.0μs and current at 23.4375A.

Figure 4.28 shows the overall results for optimization of all the four factors to attain maximum MRR and minimum TWR and Ra values.

The following conclusions are drawn from the above result:

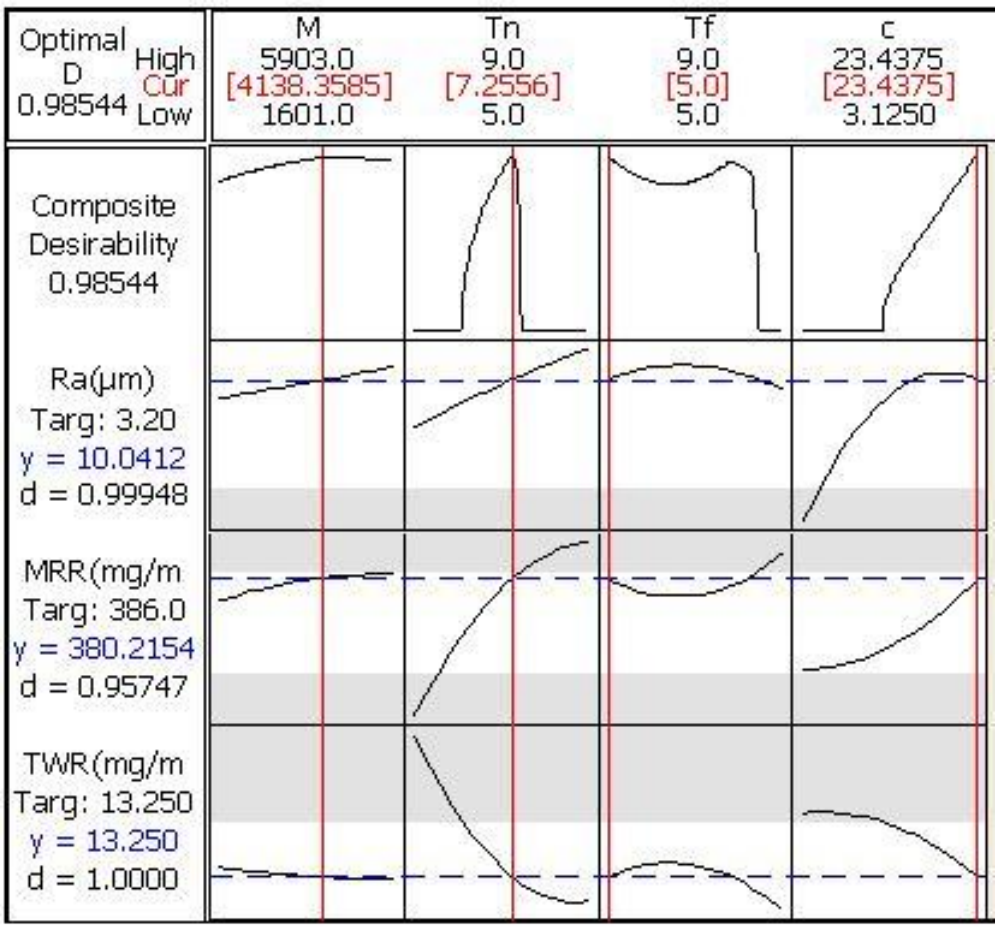

Figure 4.28: Overal statistical response optimization

1. Magnetic Intensity: Increasing this factor increases MRR and Ra responses and reduces TWR. The optimal setting is in the upper range (4138.3585G), reflecting a compromise between conflicting goals. The goal is to maximize MRR and minimize both Ra and TWR.

2. Pulse-on time: Increasing Tn also increases Ra and MRR and reduces TWR, but the effect

on Ra is minimal compared to the effect on MRR. The optimal settings of T_n is at the middle levels(7.2556μs) in the experiment.

3. Pulse-off time: Increasing Tf reduces MRR and increases TWR and Ra. At high values the reverse is true. The optimal setting is found to be at the lower values(50μs).

4. Current: Reducing current increases TWR and reduces Ra and MRR. Optimal setting is found to be at the higher range(23.4375A).

The optimal settings of current and pulse-off time are at maximum and minimum levels respectively in this research. This suggests that it might be advantageous to experiment with further extreme values for the two factors. It can be seen from the graphs that higher currents may be especially worth considering. If the graphs could be extrapolated, higher currents would improve all three responses.

Chapter 5
CONCLUSIONS AND RECOMMENDATIONS

5.1 Conclusion

This research entailed investigating the feasibility of using magnetic energy to improve the process parameters of electrical discharge machining. A precise and thorough design-of-experiment was created that allowed the relationship between these parameters(material removal rate, surface roughness and tool wear rate) and the factors of magnetic intensity, pulse-on time,current and pulse-off time be established. Thereafter the experiments were conducted and the results analysed. Empirical modelling was also done resulting in statistical formulas for mathematical acquisition of MRR,Ra and TWR for machining runs involving variation of magnetic strength,current and pulse-on and off times.

Analysis of the results verified that magnetic force improved the process parameters by increasing the rates of material removal and reducing the roughness (as a requirement for finishing operations) and tool wear rate. Finally optimum settings for the machining parameters (pulse-on and pulse off time, current and magnetic intensity)were established.

5.2 Recommendations for further research

Three main aspects can be considered for further research in relation to the optimization of the EDM process parameters under influence of magnetic energy. These include:

- Use of stronger magnetic intensities i.e. above 5903G. This can either be from permanent magnets or electromagnets.
- Variation of other factors in relation to the magnetic intensities e.g. voltage levels and pulse types.

- Use of a different type of dielectric fluid, material of the tool electrode and the workpiece.

For a long cyclic experimental setup, it would be necessary to develop an integral setup for cleaning the magnets once they are sufficiently covered by eroded debris.

References

[1] Newman S.T., "State of the art electrical discharge machining (edm)," *Int. J. Mach. Tools Manuf.*, vol. 43, pp. 1287–1300, 2003.

[2] Keskin Y. H., Halkac S. and Kizil M., "An experimental study for determination of the effects of machining parameters on surface roughness in electrical discharge machining (edm)," *International journal of advanced. Manufacturing technology.*, vol. 28, p. 11181121, 2006.

[3] Ramasawmy H. and Blunt L., "Effect of edm process parameters on 3d surface topography," *Journal of Materials Processing Technology*, vol. 148, pp. 155–164, 2004.

[4] Naotake M. and Katsushi F., "Assisting electrode method for machining insulating ceramics," *CIRP Annals Manufacturing Technology*, vol. 45, pp. 201–204, 1996.

[5] Chris J.M. and Eric R.M., "Micro machining glass with polycrystalline diamond tools shaped by micro electro discharge machining," *Journal of Micromechanics and Microengineering*, vol. 14, pp. 1687–1692, 2004.

[6] Stephen F.K. and Alber F.C., *Technology of machine tools.* Marcel Dekker Inc., New York, USA, 1997.

[7] Webzell S., *Machinery.* Findlay publications LTD, Kent UK, 2001.

[8] McGeogh J.A., *Advanced method of machining.* Chapman and Hall, London, UK, 1988.

[9] Harrold Clifford Town, *The design and construction of the machine tools.* Butterworth Co Ltd.,London England, 1971.

[10] Ghoreishi M. and Atkinson J., "A comparative experimental study of machining characteristics in vibratory, rotary and vibro-rotary electro-discharge machining," *journal of material processing technology, Manchester, UK*, vol. 120, pp. 374–384, 2002.

[11] McGeough J.A., *Advanced Methods of machinig.* Chapman & Hall, New York, 1988.

[12] Thide Bo, *Electromagnetic Field Theory.* Upsalla Sweden, 1997.

[13] Rajurkar K. and Pandit S., "Formation and ejection of EDM debris," *Transactions of the ASME*, vol. 108(2), pp. 22–26, 1988.

[14] Masuzawa T. and Taniguchi N., "Improved jet flushing for EDM," *Annals of the CIRP 41*, vol. 41, pp. 239–242, 1992.

[15] Kremer D. and Moisan A., "A study of the effect of synchronizing ultrasonic vibrations with pulse in edm," *Annals of the CIRP*, vol. 40(1), pp. 211–214, 1991.

[16] Thoe T. and Killey N., "Combined ultrasonic and electrical discharge machining of ceramic-coated nickel alloy," *Journal of Materials Processing Technology*, vol. 92-93, pp. 323–328, 1999.

[17] Lin Y., Yan.B. and Huang.F., "Surface modification of Al Zn Mg aluminum alloy using combined process of EDM with USM," *Journal of Materials Processing Technology*, vol. 115, pp. 359–366, 2001.

[18] Black S.C, *Principles of engineering manufacture.* Butterworth Heinemann, 1996.

[19] Schumacher B.M., "About the role of debris in the gap during electrical discharge machining," *Annals of the CIRP*, vol. 39, pp. 197–199, 1990.

[20] Li X.P and Lee S.H., "Study of the effect of machining parameters on the machining characteristics in electrical discharge machining of tungsten carbide," *Journal of Materials Processing Technology*, vol. 115, pp. 344–358, 2001.

[21] Yamaguchi H and Shinmura.T., "Study of an internal magnetic abrasive finishing using a pole rotation system. discussion of the characteristic abrasive behavior," *Precision Engineering*, vol. 24, pp. 237–244, 2000.

[22] Wang Y. and Hu D., "Study on the inner surface finishing of tubing by magnetic abrasive finishing," *International Journal of Machine Tools and Manufacture*, vol. 45, pp. 43–49, 2005.

[23] Kim J.D., Jin D.X. and Choi.M.S., "Study on the effect of a magnetic field on an electrolytic finishing process," *International Journal of Machine Tools and Manufacture*, vol. 37, pp. 410–408, 1997.

[24] Bruijn H.E. and Pekelharing A.J., "Effect of a magnetic field on the gap cleaning in edm," *Ann. CIRP*, vol. 27, pp. 93–95, 1978.

[25] Lin Y. C and Lee H. S., "Machining characteristics of magnetic force-assisted edm," *International Journal of Machine Tools and Manufacture*, vol. 48, pp. 1179–1186, 2008.

[26] Yeo S.H. and Cheah H.T., "Magnetic field assisted micro electro-discharge machining," *Journal of Micromechanics and Microengineering*, vol. 14, pp. 1526–1529, 2004.

[27] Croat J.J, Herbst J. F and Pinkerton F.E, "Liquid coated melt-spun NdFeB powders for bonded magnets," *Journal of Applied Physics*, vol. 55, pp. 2078–2082, 1998.

[28] Trout S. and Yuriy Z., "Effective use of neodymium iron boron magnets, case studies," *Electric Manufacturing and Coil Winding '99 Conference*, 1999.

[29] Sven Landsgesell, *Magneto-Electric Properties in Neodymium Yttrium Manganites.* Suedwestdeutscher Verlag fuer Hochschulschriften, 2010.

[30] Popa M.S., Contiu G. and Pop G., "Surface quality of the edm processed materials," *Fundamental and applied metrology*, vol. 19, pp. 1863–1866, 2009.

[31] Kumar K.L., Sivasubramanian R. and Kalaiselvan K., "Selection of optimum parameters in non conventional machining of metal matrix composite," *Portugaliae electrochimica acta.*, vol. 27, pp. 477–486, 2009.

[32] Singh S, Kansal H.K and Kumar P., "Parametric optimization of powder mixed electrical discharge machining by response surface methodology," *Journal of Materials Processing Technology*, vol. 169, pp. 427–436, 2005.

[33] Mohan B., Rajadurai A. and Satyanarayana K., "Electric discharge machining of alsic metal matrix composites using rotary tube electrode," *Journal of Materials Processing Technology*, vol. 153-154, pp. 978–985, 2004.

[34] Kansal H.K, Singh S. and Kumar P., "Effect of silicon powder mixed edm on machining rate of aisi d2 die steel," *Journal ofManufacturing Processes*, vol. 9, pp. 13–22, 2007.

[35] Saha S.K. and Chaudhary S.K., "Experimental investigation and empirical modeling of the dry electrical discharge machining process," *International Journal of machine tools and manufacturing*, vol. 49, pp. 297–308, 2009.

[36] Abu Zied O.A., "The role of voltage pulse off time in the electro discharge machined aisi t1 high speed steel," *Journal of Material process Technology*, vol. 61, pp. 287–291, 1996.

[37] Crookall J.R. and Heuvelman C.J., "Electro-discharge machining-the state of the art," *Annual of the CIRP*, vol. 20, pp. 113–120, 1971.

[38] Amorim F.L. and Weingaertnen W.L., "Influence of duty factor on the die sinking electrical discharge machining of high-strength aluminum alloy under rough machining," *Journal of Braz.soc.Mechanical Sciences*, vol. 24, pp. 194–199, 2004.

[39] *Krishna Mohan Rao, Satyanarayana G., Praveen S. :Influence of machining parameters on electric discharge machining of maraging steels-An experimental investigation, Proceeding of the world congress on Eng., Vol. II.*, 2008.

[40] Chow H.M, Yan B.H and Huang F.Y., "Micro slit machining using electro-discharge machining with a modified rotary disk electrode (rde)," *Journal of Materials Processing Technology*, vol. 91, pp. 161–166, 1999.

[41] Montgomery D.C, *Design and analysis of experiments,*. Wiley, New York, 1997.

[42] Kansal H. K, Sehijpal S. and Kumar P., "Parametric optimization of powder mixed electrical discharge machining by response surface methodology," *J. Mater. Processing Technol*, vol. 169, p. 427, 2005.

Appendix A
THEORETICAL BACKGROUND

A.1 Design of experiment

A.1.1 Response surface methods

Response surface methods (RSM) are used to examine the relationship between a response and a set of quantitative experimental variables or factors. These methods are employed in research work after identification of a vital few controllable factors influencing the performance parameters of the operation. The methods also facilitate discovery of the factor settings that optimize the response. In this research curvature in the response surface was expected and this was another reason why this techniques were chosen.

Response surface methods are employed to:

- Find factor settings (operating conditions) that produce the best response.
- Find factor settings that satisfy operating or process specifications.
- Identify new operating conditions that produce demonstrated improvement in product quality over the quality achieved by current conditions.
- Model a relationship between the quantitative factors and the response.

In RSM, it is possible to represent independent process parameters in quantitative form as:

$$Y = f(X1, X2, X3.....Xn) \pm \epsilon \tag{A.1}$$

where Y is the response (yield), f is the response function, ϵ is the experimental error, and X1, X2,X3,.....Xn are independent parameters.

By plotting the expected response of Y, a surface, known as the response surface, is obtained. The form of f is unknown and can be very complicated [41].

Thus, RSM aims to approximate f by a suitable lower ordered polynomial in some region of the independent process variables. If the response can be well modelled by a linear function of the independent variables, the function can be written as:

$$Y = C_0 + C_1X_1 + C_2X_2 + ... + C_nX_n \pm \epsilon \tag{A.2}$$

However, if a curvature appears in the system, then a higher order polynomial such as the quadratic model (equation A.3) may be used.

$$Y = C_0 + \sum_{i=1}^{n} C_iX_n + \sum_{i=1}^{n} d_i{X^2}_i \pm \epsilon \tag{A.3}$$

The objective of using RSM is not only to investigate the response over the entire factor space, but also to locate the region of interest where the response reaches its optimum or near optimal value. By studying carefully the response surface model, the combination of factors that gives the best response, can then be established [42].

Generally two response surface designs can be used: box-Behnken designs and central composite designs.

Box-Behnken designs

This is a technique for fitting quadratic models that requires 3 levels of each factor and is rotatable (or nearly rotatable). The Box-Behnken design is an independent quadratic design in that it does not contain an embedded factorial or fractional factorial design. In this design

the treatment combinations are at the midpoints of edges of the process space and at the center.This is illustrated in figure A.1. The designs have limited capability for orthogonal blocking compared to the central composite designs.

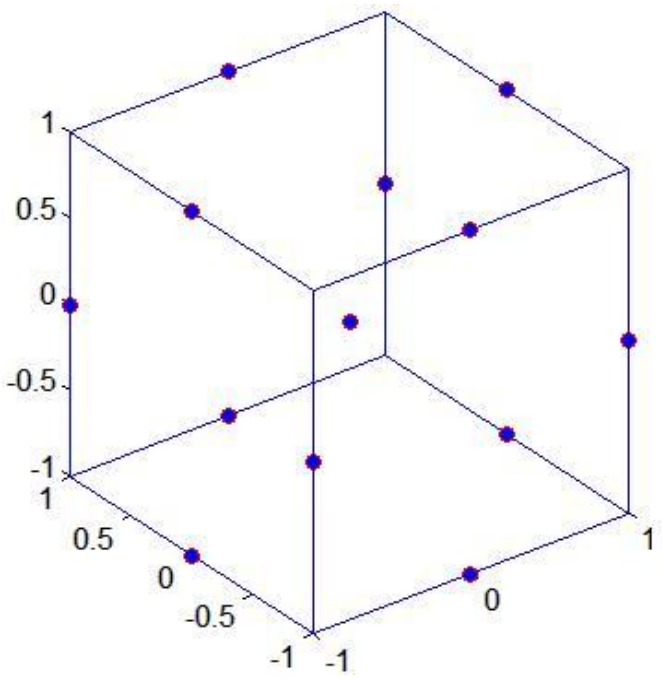

Figure A.1: Box-Behnken design

Central composite design (CCD)

A central composite design is an experimental design, useful in response surface methodology, for building a second order (quadratic) model for the response variable without needing to use a complete three-level factorial experiment.

The design consists of three distinct aspect sets:

1. A factorial or fractional design of the factors studied, each having two levels;

2. A set of center points, experimental runs whose values of each factor are the medians of the values used in the factorial portion. This point is often replicated in order to improve the precision of the experiment;

3. A set of axial points, experimental runs identical to the centre points except for one factor, which will take on values both below and above the median of the two factorial levels, and typically both outside their range.

A full factorial experiment is an experiment whose design consists of two or more factors, each with discrete possible values or levels and whose experimental units take on all possible combinations of these levels across all such factors. A full factorial design may also be called a fully crossed design. Such an experiment allows studying the effect of each factor on the response variable, as well as the effects of interactions between factors on the response variable.

A CCD design with k factors has 2k star points i.e. twice as many star points as there are factors in the design. The star points represent new extreme values (low and high) for each factor in the design.

There exists three varieties of CCDs i.e central composite circumscribed(CCC), central composite inscribed (CCI) and central composite face centered. The CCC explores the largest process space and the CCI explores the smallest process space. Both the CCC and CCI are rotatable designs, but the CCF is not. In the CCC design, the design points describe a circle circumscribed about the factorial square. For three factors, the CCC design points describe a sphere around the factorial cube.

Table A.1 summarizes the properties of the three varieties of central composite designs.

Table A.1: Varieties of central composite designs

Central Composite Design Type	Terminology	Comments
Circumscribed	CCC	CCC designs are the original form of the central composite design. The star points are at some distance from the center based on the properties desired for the design and the number of factors in the design. The star points establish new extremes for the low and high settings for all factors.
Inscribed	CCI	For those situations in which the limits specified for factor settings are truly limits, the CCI design uses the factor settings as the star points and creates a factorial or fractional factorial design within those limits (in other words, a CCI design is a scaled down CCC design with each factor level of the CCC design divided by to generate the CCI design). This design also requires 5 levels of each factor.
Face Centered	CCF	In this design the star points are at the center of each face of the factorial space. This variety requires 3 levels of each factor. Augmenting an existing factorial or resolution V design with appropriate star points can also produce this design.

The α-value is the distance of each axial point(star point) from the center in a central composite design. This value depends on the number of experimental runs in the factorial portion of the central composite design. This value, along with the number of center points, determines whether a design can be orthogonally blocked and is rotatable.

Table A.2 illustrates some typical values of α as a function of the number of factors.

Table A.2: Determining α for Rotatability

Number of Factors	Factorial Portion	Scaled Value for α Relative to $\pm$ 1
2	2^2	$2^{2/4}$= 1.414
3	2^3	$2^{3/4}$= 1.681
4	2^4	$2^{4/4}$= 2.000
5	2^{5-1}	$2^{4/4}$= 2.000
5	2^5	$2^{5/4}$= 2.378

A central composite design consists of a cube portion made up of the design points from a 2^k factorial or 2^k fractional factorial design, 2k axial or star points and center points (where k is the number of factors). Points on figure A.2 below represent the experimental runs that are performed in a 2-factor central composite design:

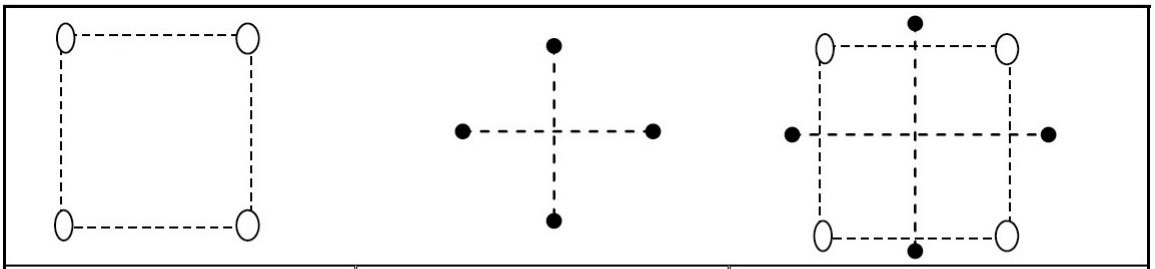

The points in the cube portion of the design are coded to be -1 and +1.	The points in the axial or star portion of the design are at (α,0),(α,0),(0,α),(0,α)	The cube and axial portions along with the center is shown. The design center is at (0, 0).

Figure A.2: Axial and center points in a CCD

Key features of this design include:

- It can incorporate information from a properly planned two-level factorial experiment

and thus recommended for sequential experimentattion.

- It allows for efficient estimation of quadratic terms in a regression model
- It exhibits the desirable properties of having orthogonal blocks and being rotatable or nearly rotatable.

A.1.2 Analysis of response surface design

Analysis of the Response Surface Design is carried out in order to fit a model to data collected using the created central composite design. A model can be fitted with linear, squared or interaction terms.

P-Values

The p-values (P) are used to determine which of the effects in the model are statistically significant. These values determine the appropriateness of rejecting the null hypothesis in a hypothesis test. It is the probability of obtaining a test statistic that is at least as extreme as the calculated value if the null hypothesis is true. The p-value is calculated from the observed sample and represents the probability of rejecting the null hypothesis when it it actually true(type I error). Study of the analysis of variance table at the p-values for the omnibus F-tests is done for all linear, all squared and all interaction effects. After identification of a significant set of effects (for example linear effects, or interaction effects), the regression table is used to evaluate the individual effects.

If the analysis of variance table suggests significant squared or interaction effects, a study of them first is conducted because they will influence the interpretation of the linear effects. To use the p-value, the following is needed:

1. Identification of the p-value for the effects to be evaluated.

2. Comparison of this this p-value to an α -level.

If the p-value is less than or equal to α, then the effect is significant. If the p-value is greater than α ,the effect is not significant.

Block, Interaction, squared and linear effects are evaluated to determine significance in the model. Squared terms are used to evaluate whether or not there is curvature (quadratic) in the response surface.

Coeffecients

For each term in the model, there is a coefficient. These coefficients are used to construct an equation representing the relationship between the response and the factors.

R-Squared

R and adjusted R represent the proportion of variation in the response that is explained by the model.

- R^2 (R-Sq) describes the amount of variation in the observed responses that is explained by the model. It is a percentage of response variable variation that is explained by its relationship with one or more predictor variables. The higher the R^2, the better the model fits the data.
- Predicted R^2 reflects how well the model will predict future data.
- Adjusted R^2 is a modified R^2 that has been adjusted for the number of terms in the model. If unnecessary terms are included, R^2 can be artificially high. Unlike R^2 , adjusted R^2 may get smaller when terms are added to the model.

Appendix B

EXPERIMENTAL RESULTS FOR RUNS WITHOUT MAGNETIC INFLUENCE

Table B.1: Experimental results: Runs without magnetic influence

Expt No.	$T_n(\mu s)$	I(A)	$T_{off}(\mu s)$	TWR(mg/min)	Ra(μm)	
1.	60	21.875	80	220.00	19.32	10.429
2.	80	21.875	80	310.01	18.33	12.17
3.	80	9.375	60	220.12	14.67	9.5
4.	60	9.375	60	219.12	13.09	9.3
5.	60	9.375	60	190.01	16.37	9.0
6.	80	21.875	60	243.01	18.61	10.5
7.	60	21.875	80	290.11	14.67	9.5
8.	70	15.625	50	210.02	19.92	13.2
9.	70	15.625	70	209.12	11.99	12.97
10.	70	15.625	70	213.12	15.01	10.61
11.	60	9.375	80	220.09	19.97	11.21
12.	60	21.875	60	221.12	16.63	11.3
13.	50	15.625	70	214.21	17.09	11.0
14.	80	21.875	60	221.91	16.76	11.01
15.	70	15.625	70	240.12	16.68	11.97
16.	80	9.375	60	167.00	17.97	10.7
17.	70	15.625	70	232.12	12.19	12.21
18.	80	9.375	80	312.00	16.67	11.2
19.	80	21.875	80	312.11	16.25	14.72
20.	70	15.625	70	268.01	16.87	12.21
21.	70	15.625	70	276.00	18.05	11.61
22.	60	9.375	80	243.12	16.11	10.21
23.	70	3.125	70	301.12	16.33	8.5
24.	80	9.375	80	301.00	17.33	13.12
25.	60	9.375	60	209.09	17.99	8.90

Appendix C

ANOVA OVERVIEW

Analysis of variance (ANOVA) is a collection of statistical models used to analyze the differences between group means and their associated procedures (such as "variation" among and between groups). In ANOVA setting, the observed variance in a particular variable is partitioned into components attributable to different sources of variation. In its simplest form, ANOVA provides a statistical test of whether or not the means of several groups are equal, and therefore generalizes t-test to more than two groups. Doing multiple two-sample t-tests would result in an increased chance of committing a type I error. For this reason, ANOVAs are useful in comparing (testing) three or more means (groups or variables) for statistical significance.

ANOVA is a particular form of statistical hypothesis testing heavily used in the analysis of experimental data. A statistical hypothesis test is a method of making decisions using data. A test result (calculated from the null hypothesis and the sample) is called statistically significant if it is deemed unlikely to have occurred by chance, assuming the truth of the null hypothesis. A statistically significant result (when a probability (p-value) is less than a threshold (significance level)) justifies the rejection of the null hypothesis.

In the typical application of ANOVA, the null hypothesis is that all groups are simply random samples of the same population. This implies that all treatments have the same effect (perhaps none). Rejecting the null hypothesis implies that different treatments result in altered effects.

By construction, hypothesis testing limits the rate of Type I errors (false positives leading to false scientific claims) to a significance level. Experimenters also wish to limit Type II errors

(false negatives resulting in missed scientific discoveries). The Type II error rate is a function of several things including sample size (positively correlated with experiment cost), significance level (when the standard of proof is high, the chances of overlooking a discovery are also high) and effect size (when the effect is obvious to the casual observer, Type II error rates are low).

The terminology of ANOVA is largely from the statistical design of experiments. The experimenter adjusts factors and measures responses in an attempt to determine an effect. Factors are assigned to experimental units by a combination of randomization and blocking to ensure the validity of the results. Blinding keeps the weighing impartial. Responses show a variability that is partially the result of the effect and is partially random error.

ANOVA is the synthesis of several ideas and it is used for multiple purposes. As a consequence, it is difficult to define concisely or precisely.

Classical ANOVA for balanced data does three things at once:

1. As exploratory data analysis, an ANOVA is an organization of an additive data decomposition, and its sums of squares indicate the variance of each component of the decomposition (or, equivalently, each set of terms of a linear model).

2. Comparisons of mean squares, along with F-tests ... allow testing of a nested sequence of models.

3. Closely related to the ANOVA is a linear model fit with coefficient estimates and standard errors.

   ANOVA uses traditional standardized terminology. The ANOVA table is structured to

outlay the various statistical derivations.The SS column represents the sum of squared deviations for each of several different ways of choosing which deviations to look at, and these are labeled Source (of Variation) .Each SS has a corresponding df (degrees of freedom) which is a measure of the number of inde- pendent pieces of information present in the deviations that are used to compute the corresponding SS And each MS is the SS divided by the df for that line. Each MS is a variance estimate or a variance-like quantity, and as such that its units are the squares of the outcome units.